Geomorphology 415 (2022) 108411

Contents lists available at ScienceDirect

Geomorphology

journal homepage: www.journals.elsevier.com/geomorphology

Estimating the long-term slip rate of active normal faults: The case of the Paganica Fault (Central Apennines, Italy)

Irene Puliti [a,b,*], Stefano Pucci [c], Fabio Villani [c], Massimiliano Porreca [b], Lucilla Benedetti [d], Gaetano Robustelli [e], Anna Gueli [f], Giuseppe Stella [f]

[a] Dipartimento di Ingegneria e Geologia, Università di Chieti-Pescara "G. d'Annunzio", Via dei Vestini 31, 66100 Chieti, Italy
[b] Dipartimento di Fisica e Geologia, Università di Perugia, Piazza dell'Università, 00123 Perugia, Italy
[c] Istituto Nazionale di Geofisica e Vulcanologia, Via di Vigna Murata 605, 00143 Rome, Italy
[d] Aix-Marseille Université, CNRS-IRD-Collège de France UMR 34 CEREGE, Aix en Provence, France
[e] Dipartimento di Biologia, Ecologia e Scienze della Terra, Università della Calabria, Via P. Bucci, Cubo 15B, 87036 Arcavacata di Rende (CS), Italy
[f] PH3DRA labs, Dipartimento di Fisica e Astronomia E.Majorana dell'Università and INFN, via Santa Sofia 64, 95123 Catania, Italy

ARTICLE INFO

Keywords:
Active faults
Earthquake geology
L'Aquila earthquake
Morphotectonics

ABSTRACT

The footwall of the surface rupturing Paganica normal fault, the source of the 2009 L'Aquila earthquake (Mw 6.1) in the Central Apennines (Italy), was investigated using integrated geological and geomorphological approaches. The aim was to constrain the active tectonics by studying the Raiale River that orthogonally crosscuts the fault trace, where it provides a useful geomorphological marker of long-term fluvial incision and footwall uplift. Using morphostratigraphy and paleomagnetic analysis, the Plio–Pleistocene morphotectonic evolution of the area was reconstructed, comprising an ancient continental basin and paleolandforms that predate the footwall incision. Starting from the Late Early Pleistocene–Middle Pleistocene, fluvial dissection was mainly due to marked river downcutting triggered by significant activity of the Paganica Fault, which caused progressive base-level lowering. The Raiale River downcutting formed five Middle–Late Pleistocene fluvial terraces, that, along with absolute Optically Stimulated Luminescence (OSL) dating, allowed the identification of paleolongitudinal profiles with a diverging downstream configuration. Terrace dating yielded a minimum incision rate of 0.25 ± 0.02 mm/a, which only partially compensates the footwall uplift and can thus be considered as a minimum value for the Paganica Fault throw rate, which could reach up to ~0.45 mm/a. In parallel, using terrestrial cosmogenic nuclides, a denudation rate of 0.02–0.04 mm/a was measured on the summit of the footwall block. This denudation is in keeping with the drainage incision, suggesting a non-steady state for the fault footwall topography and a dominance of relief growth. Last, the analysis of the modern Raiale River longitudinal profile denoted an ungraded status, with two main knickzones that we interpret as transient forms due to tectonic perturbations, likely triggered by activity of the Paganica Fault during the end Early Pleistocene and the Late Pleistocene. Considering the 2009 L'Aquila earthquake coseismic rupture, we observe that the younger transience on the Raiale River longitudinal profile, if it is of tectonic origin, could have only been produced by much larger seismic events (i.e., Mw > 6.5) than those documented in the area by paleoseismological investigations. The collective results confirmed that in the Central Apennines, conditions of dynamic equilibrium are often not met, and that the persistence of transient perturbations induced by tectonics should be accounted for.

1. Introduction

In actively deforming areas, landscapes are affected by the interactions between tectonic and climatic changes (Bull, 2011) and undergo erosion and deposition that drive the shape of the topography (Kirby and Whipple, 2012). Overall, drainage systems are susceptible to the external tectonic and climatic factors that may trigger variations on the rivers' concave longitudinal profile in the topographic steady state (i.e., graded or equilibrium profile; Chorley and Kennedy, 1971; Ahnert, 1994; Zhou et al., 2017). Rivers can have small fluctuations over many decades that reflect the short-term changes of boundary conditions, mostly linked to climate (e.g., flow rate and sediment load; Whittaker

* Corresponding author at: Dipartimento di Ingegneria e Geologia, Università di Chieti-Pescara "G. d'Annunzio", Via dei Vestini 31, 66100 Chieti, Italy.
E-mail address: irene.puliti@unich.it (I. Puliti).

https://doi.org/10.1016/j.geomorph.2022.108411
Received 12 October 2021; Received in revised form 12 August 2022; Accepted 15 August 2022
Available online 17 August 2022

et al., 2007a; Pazzaglia, 2003; Pérez-Peña et al., 2010). This contrasts with local and regional tectonic forces that can lead to more major perturbations on the river graded profile through fault-block movements or isostatic adjustments.

In bedrock dominated (detachment-limited) river channels, the lowering of the base level (and/or uplift) drives the development of a knickpoint/knickzone. This results in a transient state with an ungraded longitudinal profile (Merritts and Vincent, 1989; Whipple and Tucker, 1999; Wobus et al., 2006; Berlin and Anderson, 2007), where the upstream migration of a knickpoint/knickzone represents a regressive wave of incision that progressively restores the equilibrium state through incision or aggradation (Tucker and Whipple, 2002; Harkins et al., 2007; Whittaker et al., 2010).

When tectonic uplift (or subsidence) is balanced by incision (or sedimentation), such quasi-equilibrium conditions (i.e., graded profile) are met. However, this only occurs if the timescale of tectonic changes is larger than the timescale of the channel response. Conversely, if, for example, the rate of footwall uplift due to coseismic surface faulting (hence, the slip per event/recurrence time) exceeds the mean rate of river incision, the ungraded longitudinal profile is preserved in the long term.

Based on this evidence, several studies were published on how the role of tectonics can be independently determined by the theoretical drainage transient response to uplift rate variations (e.g., Whipple and Tucker, 1999, 2022; Snyder and Hodges, 2000; Kirby and Whipple, 2001; Wobus et al., 2006; Cyr et al., 2010; Pucci et al., 2014; De Gelder et al., 2019). Specifically, rivers counterbalance the footwall uplift of active normal faults and incise valleys (Hancock and Anderson, 2002; Starkel, 2003; Azañón et al., 2005), providing an opportunity to create and preserve relict fluvial landforms through which paleolongitudinal profiles can be reconstructed. These paleolongitudinal profiles represent timelines that are helpful for deducing the evolution of base-level changes and are a valuable tool for estimating the uplift rates (Schumm, 1993; Bogaart and Van Balen, 2000; Hetzel et al., 2002; Watchman and Twidale, 2002; Pérez-Peña et al., 2009). We use this theory as a tool for analyzing the long-term tectonic activity of a key earthquake prone fault in the Apennines of Central Italy.

In this study geomorphological and Quaternary geological investigations are combined to extract tectonic signals from the incisional history of the Raiale River in the Abruzzi region (Central Italy). The study area includes the upper reach of the Raiale River that flows on the uplifting footwall and crosses the active Paganica normal fault. This fault is responsible for the major 2009 L'Aquila earthquake (Mw 6.1), which produced surface coseismic faulting and caused considerable damage and fatalities (Emergeo Working Group, 2009; Pondrelli et al., 2010; Scognamiglio et al., 2010; Herrmann et al., 2011).

This study focused on two elements: (1) reconstruction of the Quaternary evolution of the area, supported by chronological constraints of the continental deposits, with emphasis on the fluvial history, to unravel depositional and erosional processes that occurred at the footwall of the Paganica Fault as a response to local tectonic forcing and (2) estimation of an independent long-term throw rate of the Paganica Fault for comparison with near-fault measurements made with other techniques (Galli et al., 2010; Boncio et al., 2010; Roberts et al., 2010; Cinti et al., 2011; Moro et al., 2013; Villani et al., 2017; Civico et al., 2017).

To achieve these, a combination of field surveys of Quaternary continental and Late Pleistocene–Holocene fluvial terrace deposits with paleomagnetic and optically stimulated luminescence (OSL) dating techniques was performed. The morphostructural reconstruction of depositional bodies and erosional landforms was performed by integrating different datasets from aerial photos and high-resolution topography (LiDAR-derived digital elevation model (DEM)) interpretations.

The long-term activity (i.e., throw rate) of the Paganica Fault was obtained by investigating the adjustment of the Raiale River longitudinal profile to ongoing footwall uplift by channel incision. Specifically, with a hypothesis that the Raiale River tends to a topographic steady state (i.e., equilibrium) through a transient response to tectonic perturbation, the channel incision rate approaches the rate of tectonic uplift. In agreement with the theoretical models of normal faults (Lavé and Avouac, 2001), the maximum footwall uplift occurs at the surface trace of the Paganica Fault, as shown by the surface rupture patterns from InSAR data after the 2009 earthquake (Atzori et al., 2009). Thus, near the fault, in correspondence with the lower drainage reaches (i.e., the main stem), we also expect the most significant channel incision rates. Particular attention was given to mapping and dating the fluvial terrace flights preserved along the upper reach of the Raiale River as evidence of paleo-thalweg levels and progressive channel downcutting to acquire a reliable river incision rate.

The denudation rate was measured at the summit of the drainage incising the footwall block using cosmogenic exposure dating to evaluate the landscape sensitivity to the disturbing tectonic forces. Collectively, the results were considered alongside published data on the long-term and 2009 L'Aquila earthquake activity of the Paganica Fault, which are produced through independent methodologies. Finally, the effect of fault activity on the landscape relief dynamics is discussed.

2. Seismotectonic and geological setting

The study area is in the axial sector of the Central Apennines, a NE-verging Neogene fold-and-thrust belt developed along the Adriatic microplate's margin and affected by multiphased contractional extensional deformation (Carminati and Doglioni, 2012). Following the subaerial summit exposure that occurred during the Messinian–Early Pliocene >5 Ma ago (Bosi et al., 2003; Centamore et al., 2006), a post-orogenic Pliocene–Quaternary extension dissected the compressional structure, mainly by NW-striking and SW-dipping normal faults. These normal faults are arranged into systems, generally not exceeding 30 km in length (Galadini and Galli, 2000; Boncio et al., 2004a, 2004b; Roberts and Michetti, 2004), showing evidence of Late Pleistocene–Holocene surface-rupturing earthquakes (Galli et al., 2008; Benedetti et al., 2013). The present-day active NE-trending extension predominantly occurs along the axis of the chain, as displayed by upper crustal instrumental seismicity (Chiarabba et al., 2005; Bagh et al., 2007; Pondrelli et al., 2010; Rovida et al., 2016) and geodetic horizontal velocities of ~1–3 mm/a (Hunstad et al., 2003; D'Agostino et al., 2011; Devoti et al., 2011; Carafa and Bird, 2016). Along the Apennines chain, the active normal fault systems controlled the evolution of the intermontane basins developed in their hanging walls and infilled with Plio–Quaternary continental deposits (Cavinato and Celles, 1999). These basins represent a geological archive of past tectonic events and climatic fluctuations, which occurred in a setting characterized by a large-scale uplift since the Early–Middle Pleistocene (D'Agostino et al., 2001).

2.1. Geological setting of the Plio–Quaternary Middle Aterno Basin

The Middle Aterno Valley (MAV) is one of the main intermontane tectonic basins in the Central Apennines. It was an initially isolated Plio–Quaternary continental depression, which became fluvially integrated into the Aterno River system and the Adriatic coast during the late Early–Middle Pleistocene (Geurts et al., 2020). The MAV is controlled by the long-term activity of a composite network of right-stepping normal fault segments generally trending NW and dipping to the SW. This fault system is known as the Paganica-San Demetrio Fault System (PSDFS) and it is mainly composed of two major faults that define this active fault array, namely, the Paganica (PAG) to the north–west, and the San Giovanni (SAG) Faults to the south–east (Galli et al., 2010; Lavecchia et al., 2012; Civico et al., 2015; Giaccio et al., 2012; Pucci et al., 2019).

This region has a strong seismogenic potential, attested by instrumental earthquakes (Pace et al., 2006; Pondrelli et al., 2010; Scognamiglio et al., 2010; Peruzza et al., 2011; Herrmann et al., 2011) and

historical reports (Terulliani et al., 2009). The PAG ruptured during the 2009 Mw 6.1 earthquake (Atzori et al., 2009; Pondrelli et al., 2009; Papanikolaou et al., 2010; Valoroso et al., 2013), causing primary surface faulting with coseismic throws up to ~15 cm, consistent with the SW-dipping geometry and kinematics of the main fault plane (Emergeo Working Group, 2009; Boncio et al., 2010) (Fig. 1). Coseismic deformation was also observed in the far-field through the Envisat and COSMO-SkyMed DInSAR interferograms that recorded a maximum footwall uplift of 5–10 cm (Atzori et al., 2009). Paleoseismic data also record recurrent Holocene ruptures along the PSDFS with an average recurrence time of ~300–500 years and 1000–2000 years for 2009-like and Mw > 6.5 events, respectively (Galli et al., 2011; Cinti et al., 2011; Moro et al., 2013; Blumetti et al., 2017). The paleo-faulting events produced throws larger (i.e., ~50 cm) than those occurred in 2009 (Cinti

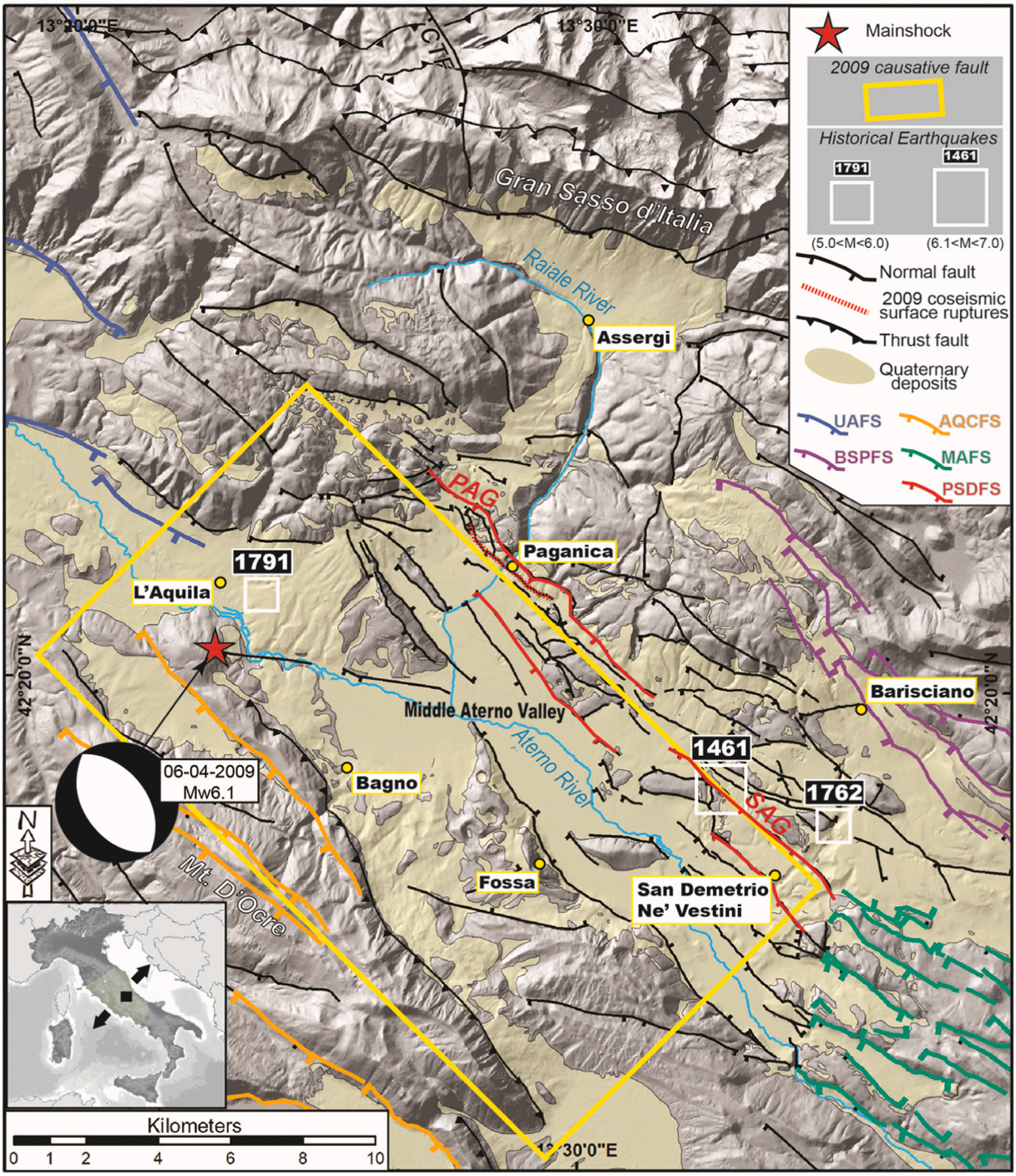

Fig. 1. Location map of the 2009 L'Aquila mainshock (Scognamiglio et al., 2010; Herrmann et al., 2011). Focal mechanisms of the mainshock, historical seismicity (Mw > 5.0, open squares; https://emidius.mi.ingv.it/CPTI15-DBMI15/), and main surrounding active fault systems are shown (acronyms as follows: UAFS, Upper Aterno Fault System; PSDFS, Paganica-San Demetrio Fault System, of which PAG and SAG are the main fault segments; BSPFS, Barisciano-San Pio Fault System; MAFS, Middle Aterno Fault System (modified after Galadini and Galli, 2000; Civico et al., 2015; Pucci et al., 2015). According to several investigators, the yellow box is the approximate projection to the surface of the ~19-km-long 2009 mainshock causative fault (Vannoli et al., 2012; Chiaraluce, 2012). DEM from 10-m resolution TIN-Italy (Tarquini et al., 2012). (For interpretation of the references to colour in this figure legend, the reader is referred to the web version of this article.)

et al., 2011; Moro et al., 2013).

The tectonic-sedimentary evolution of the MAV Basin results from the interplay of early E–W- and N–S-trending conjugate faults and the main NW–SE-trending normal fault systems (Blumetti et al., 2013; Pucci et al., 2019) (Fig. 2). This interplay prompted a compound continental deposit infilling (Ge.Mi.Na, 1963; Bertini and Bosi, 1993; Messina et al., 2001; Bosi et al., 2003; Angelino et al., 2010; Tallini et al., 2012; Giaccio et al., 2012; Spadi et al., 2016; Nocentini et al., 2018; Pucci et al., 2019), with isolated depocenters thickening up to 500–600 m (Cesi et al., 2010; Balasco et al., 2011; Improta et al., 2012; Villani et al., 2015, 2017; Santo et al., 2014; Pucci et al., 2016; Porreca et al., 2016; Civico et al., 2017).

Based on Giaccio et al. (2012) and Pucci et al. (2019) studies, the conjugated E–W and N–S-trending faults during the Late Pliocene–Early Pleistocene mostly controlled the oldest sedimentary traps, characterized by syntectonic deposition, thickness variability, and hiatuses. Most of the old infill is composed of widespread mass-wasting deposits of typical proximal facies, mainly composed of slope-breccias and rock-slide deposits (Valle Valiano Breccia Fm. -VVB, Megabreccia Fm. -MEB, Cesarano Breccia Fm. -CEB, L'Aquila Breccia Fm. -LAB) and sparse alluvial fan conglomerates (Valle Valiano Conglomerates Fm. -VVC) (Pucci et al., 2019). During the Late Pliocene–Early Pleistocene, extensive lacustrine and SE-flowing fan delta deposition (San Nicandro Fm. -SNL, and Vall'Orsa Conglomerates Fm. -VOC, respectively) occurred. Spadi et al. (2016) reported evidence of the late Piacenzian age fossils, witnessing possible older inception of the SNL lacustrine environment. Later, the NW-trending fault set became predominant at the end of the Early Pleistocene. Consequently, a prominent ~19-km-long fault system (PSDFS) dissected the proto-MAV, bounding the 3–6-km-wide Paganica-San Demetrio Basin. This kinematic change likely promoted a drastic reorganization of the fluvial system, inducing a prevailing SW-flowing alluvial fan deposition (Valle Inferno Fm. -VIC, San Mauro Fm. -SMA, ALP and ALH Fms.; Bagnaia et al., 1992; Giaccio et al., 2012; Nocentini et al., 2018; Pucci et al., 2019).

In the northern sector of the Paganica-San Demetrio Basin, the PAG, along with its set of subparallel normal fault splays, acted as the leading strand in accruing most of the long-term displacement of the PSDFS (~650 m of cumulative net throw; Pucci et al., 2016; Villani et al., 2017). The long-term subsidence of the PAG hanging wall triggered the aggradation of the >80-m-thick alluvial fans of the Raiale River, ranging in age from the Middle Pleistocene to the Holocene (Galli et al., 2010; Giaccio et al., 2012) and showing evident Middle Pleistocene syntectonic growth as suggested by high-resolution seismic data (Villani et al., 2017). In addition, the uplift of the PAG footwall block caused the

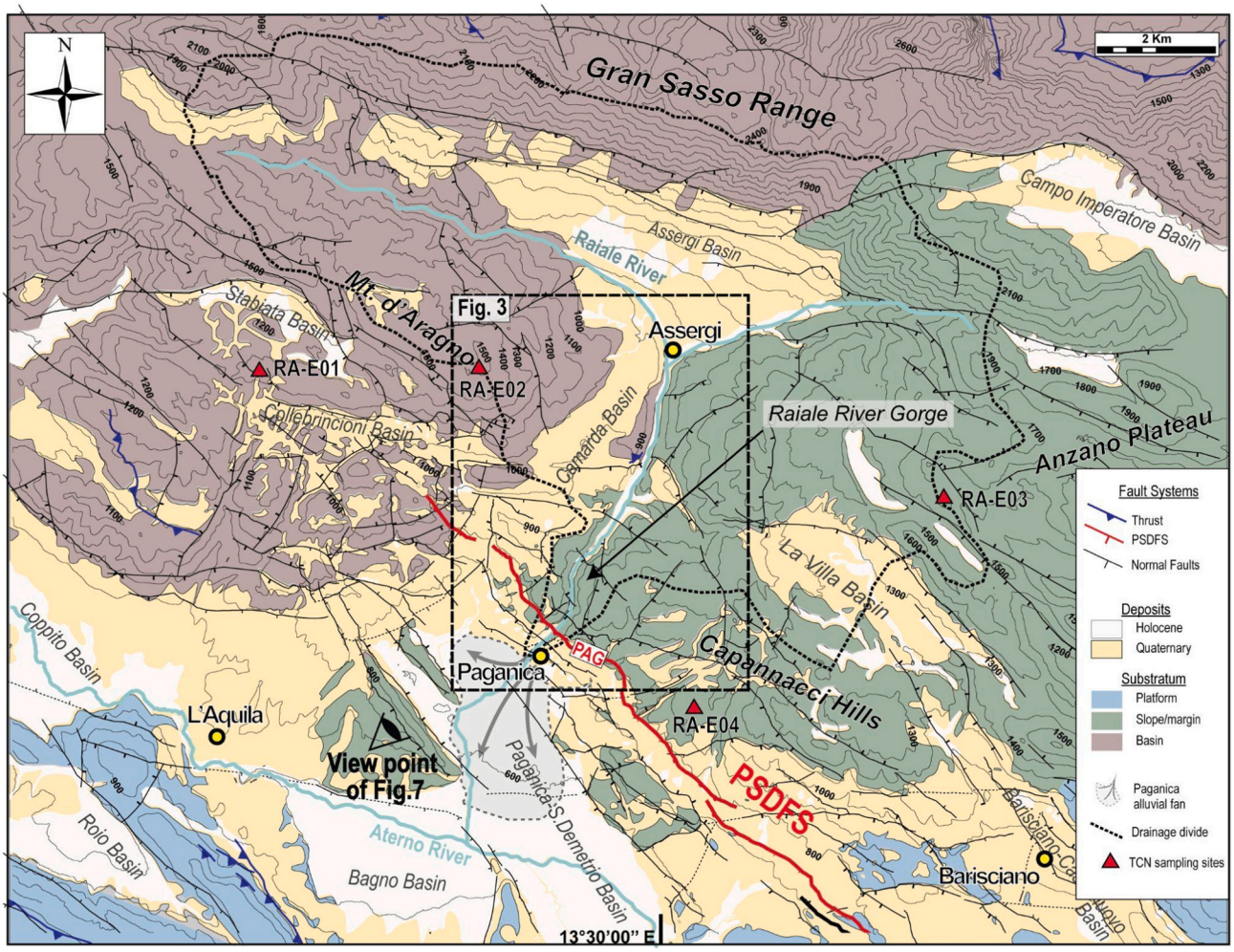

Fig. 2. Structural map of the study area (modified after Pucci et al., 2019). The NW-trending and the conjugated W- and N-trending normal faults are in black. The PSDFS is shown with a thick red line. The PAG segment is labeled. Thrust faults are in blue. The three main substratum paleogeographic domains are indicated with different colors: Umbria-Marche basinal domain and Latium-Abruzzi platform and margin domains (Centamore et al., 2006). The Holocene and Plio–Pleistocene continental deposit locations are outlined, together with the major catchment divide of the Paganica alluvial fan and the Raiale River. The red triangles indicate the sites of sampling for Terrestrial Cosmogenic Nuclides dating. (For interpretation of the references to colour in this figure legend, the reader is referred to the web version of this article.)

development of the deep gorge along the Raiale River's upper reach, wind gaps, elevated erosional surfaces, and the beheaded toes of Pliocene–Early Pleistocene breccia bodies of the Camarda Basin (Pucci et al., 2019) (Fig. 2). Paleoseismological, geophysical, and morphotectonic studies on the PAG (Galli et al., 2010; Boncio et al., 2010; Roberts et al., 2010; Cinti et al., 2011; Moro et al., 2013; Macrì et al., 2016; Villani et al., 2017; Civico et al., 2017) suggested long-term throw rates of 0.1–0.4 mm/a for the last 1–2 Ma, 0.5 mm/a for the last 450 ka, and 0.1–0.3 mm/a for the last 30 ka.

3. Materials and methods

To depict the Quaternary evolution of the landscape at the footwall block of the active Paganica Fault and to evaluate how its activity contributed to this evolution, a combination of field surveys, morphometric analysis, and dating of Quaternary deposits and landforms were conducted.

3.1. Quaternary geological map

To define the Quaternary evolution of the PAG's footwall, a tectonic and stratigraphic framework was reconstructed, from which geomorphic and depositional markers of long-term incision, denudation, and fault displacement can be deciphered. First, a detailed mapping of continental deposits and tectonic structures was performed through field surveys, aerial photo interpretation from 1:33,000 scale stereo pairs (Istituto Geografico Militare - Gruppo Aereo Italiano flights, 1954–1955), and raster imagery (Orthophoto Regione Abruzzo 2007). The applied morphostratigraphic analysis benefited from a DEM (5.0 m/pixel size, from topographic data) and a high-resolution (1.0 m/pixel size) digital surface model (DSM). The latter comes from processing airborne lidar data acquired by the Civil Protection of Friuli Venezia Giulia Region a few days after the 2009 L'Aquila earthquake (using an Optech Airborne Laser Terrain Mapper System; Civico et al., 2015).

The resulting map integrates and updates the Quaternary geological mapping of Pucci et al. (2015 and 2019), which covers a limited portion of the PAG's footwall block. In particular, this study focuses on the geometry, extent, and arrangement of the poorly known continental sequence infilling the Camarda Basin and the cross-cutting relationships of Quaternary faults with the inset deposits of the Raiale River valley. The stratigraphy of the pre Plio–Quaternary bedrock follows the subdivision proposed by the Geological Map of Italy, scale 1:50,000 (sheets 359 L'Aquila and 349 Gran Sasso; Adamoli et al., 2012), without internal subdivision. The Quaternary stratigraphy is based on the scheme proposed by Pucci et al. (2019), integrated with original geological field data.

3.2. Geomorphological analysis

The study was conducted with morphometric analysis to individuate detailed fluvial and alluvial landforms useful to constrain paleobase levels.

First, using the 5-m DEM, we extracted the longitudinal topographic profile of the Raiale River and investigated its shape and channel steepness index (K_{sn}) using the dedicated MATLAB-based software for topography analysis (TopoToolBox; Schwanghart and Scherler, 2014) and Stream Profiler (a free routine for MATLAB in ArcGIS, from Wobus et al., 2006). K_{sn} is a geomorphic index estimated by normalizing the drainage area of a given reach and using a reference concavity that corresponds to the regional concavity observed in reaches unperturbed by tectonic signals (Wobus et al., 2006). This analysis allowed the detailed reconstruction of the present-day Raiale River talweg longitudinal profile, its features (e.g., knickpoint/knickzone), and the reconstruction of the profiles prior to knickpoint propagation.

Afterward, fluvial terrace surfaces were identified along with their inner (i.e., the junction between the terrace tread and the valley slope) and outer edges (i.e., the junction between the terrace tread and the talweg riser), remnants of alluvial fans, paleosurfaces, paleovalleys, and wind gaps, stream entrenchments and gullies, and tectonic escarpments through the high-resolution DEM and its derivative slope and hillshade maps (through ArcGIS software tools).

Particular attention was paid to identifying and correlating fluvial terraces that flank the lower section of the Raiale River valley as remnants of the former talweg of the main stem. Afterward, the mapped fluvial terraces were checked in the field to assess their strath- or fill-nature. Since colluvial and slope deposits may affect the measurements of the terrace risers, by burying the inner edges of the terraces, we correlated the outer terrace edges based on surface morphology, lateral continuity, and altimetric distribution to define different levels of alluvial surfaces. Elevations of river terrace features have been projected onto a common baseline given by the smoothed longitudinal profile of the Raiale River. Profile smoothing was achieved using spatial analyst tools in ArcGIS to highlight only the main long-wavelength features in the profile, minimizing some possible unwanted features (i.e., small engineered dams). The elevation values assigned to each terrace feature represent the key elevation (i.e., the dominant elevation) of the outer edge (i.e., the intersection between the terrace tread and the talweg riser). After the projection of the terrace flight above the baseline, the correlation of the different levels of terraces has been obtained through the construction of a linear trendline. Aware of the simplifying assumption of a nearly constant-slope geomorphic marker, a linear correlation was used between terrace remnants in the middle–lower course of the Raiale Valley. In fact, our data indicate that this is a good approximation that well reproduces the general trend of the terrace. Only correlations with coefficient values $R2 > 0.8$ were retained.

3.3. Incision and denudation rate estimate

In continental extensional settings, erosional or depositional processes at fault footwall and hanging wall blocks result from the interplay between slip rates and large-scale regional uplift or subsidence rates (Bull, 2008). Since, in the Central Apennines, the normal fault footwall uplift rate is superimposed onto regional uplift (D'Agostino et al., 2001), the footwall area is dominated by erosional processes. Here, along with gravitational phenomena (Hippolyte et al., 2006), channel incision, hillslope, and summit denudation work together in landscape modeling.

To unravel the contribution of the PAG fault activity in landscape building and to reconstruct its long-term throw rate, denudation and incision rates at the footwall block were estimated and compared.

The incision rate estimate of the Raiale River is based on the elevation and age of the lowest paleolongitudinal profile. This was directly dated by sampling its terraced deposit using the OSL dating methodology (Section 3.4). The ages of other terraces were inferred by correlation with the oxygen isotope stages (OISs) curve of Lisiecki and Raymo (2005) in the hypothesis of quasi-constant incision rate through time. We tested such a correlation of the age of the fluvial terrace with the OIS because of their climatic origin, as suggested by the paleoclimatic studies of Giraudi (2005) on the nearby Gran Sasso Massif and by geomorphological studies in the broader Apennines (Coltorti et al., 1991; Wegmann and Pazzaglia, 2009; Nesci et al., 2012). Specifically, terrace deposition mainly occurs in correspondence with glacials (i.e., cold periods), when alluvial sedimentation increases due to enhanced degradation processes, whereas, during interglacials (i.e., temperate-warm periods), widespread vegetation prevents the significant transport of sediment load, and streams cut down into the alluvial sediments.

The denudation rate was determined at the summits (i.e., watershed and interfluves) of the Raiale River drainage basin using in situ produced cosmogenic nuclide ^{36}Cl measurements (Dunai, 2010; Ryb et al., 2014; Godard et al., 2016). The in situ produced ^{36}Cl cosmogenic nuclide (half-life 301 ka) is the product of the interaction between cosmic particles and mainly Ca atoms in limestones (Schimmelpfennig et al., 2011). Four sites were sampled on the carbonate paleosurface at the interfluve edges

of the Raiale Basin in the vicinity of the PAG fault trace. Such smoothed summits represent remnants of the oldest land surfaces (possibly related to the oldest Apennines subaerial exposure), which are less affected by fluvial headward erosion.

First, samples were crushed and sieved. Only the fraction of rock whose diameter was between 250 μm and 1 mm was used in the chemical preparation. Afterward, the rock samples were treated, and ^{36}Cl precipitation was obtained. Finally, we measured the concentrations of these precipitates by accelerator mass spectrometry (AMS) at the French CEREGE institute in Aix en Provence, and the denudation rates were obtained according to the procedure by Schimmelpfennig et al. (2009). The measured ^{36}Cl concentrations were determined in the AMS and normalized to a standard prepared by K. Nishiizumi (KNSTD1600, with a nominal $^{36}Cl/^{35}Cl$ value of $2.11 \pm 0.06 \times 10^{-12}$; Sharma et al., 1990; Fifield et al., 1990). The analytical uncertainties include counting statistics, machine stability, and blank correction. Last, the incision rates of the Raiale River valley and the denudation of the nearby summit were compared to provide a picture of the PAG footwall block landscape evolution.

3.4. Dating methods

To constrain the age of the Quaternary deposits and better understand their stratigraphic relations based on outcrop conditions and preservation of rock material, six sites suitable for dating with OSL and paleomagnetic analysis were chosen. Here, the following dating methods to cover different age ranges were applied: (1) paleomagnetic analysis on 62 samples collected over five sites and (2) OSL on one sample/site.

Paleomagnetic analysis was performed at the Paleomagnetism Laboratory of the Istituto Nazionale di Geofisica e Vulcanologia (INGV) in Rome to infer the age of the old breccia deposits. The measurement of the natural remaining magnetization of the rock sample has been undertaken using a cryogenic magnetometer 2G based on the superconductivity of helium liquid. Each set of samples was organized into two subsets to obtain accurate measures, and two different methods were used to demagnetize them: thermal demagnetization and alternate field according to methods described by Messina et al. (2001) and Saroli et al. (2015). Five sites were chosen based on morphostratigraphic relationships, and samples were drilled in the field using a gasoline-powered drill, one for each breccia deposit (Fig. 3). The target breccia or conglomerate deposits are characterized by a significant percentage of the fine-grained and cemented matrix as it is the only component of these continental deposits able to be magnetized during sedimentation. The main magnetic components for each site were analyzed using Remasoft software from which the paleomagnetic mean vector representing the magnetization was calculated (i.e., magnetic polarity; Chadima et al., 2006). Subsequently, the magnetic polarity of the sampled sequence was ascribed to the time scale through the stratigraphic relationships of the sampled deposits.

OSL techniques were performed to date the fluvial deposits composed of quartzitic fine layers. Standard sampling techniques were utilized for poorly lithified materials, sampling by hammering a 15-cm-long aluminum tube into a silty–sandy layer at 0.7 m from the vertical outcrop cut and 1.0 m from the surface of the tread, with ~1.0 kg of sediment collected for dose rate measurement. Sample preparation and OSL (Aitken, 1982) were conducted at the PH3DRA laboratory of the Department of Physics and Astronomy "E. Majorana", University of Catania (Italy) Equivalent Dose (ED) rates were obtained from the extracted coarse-grained quartz fraction through single-aliquot regenerative-dose protocol (Murray and Wintle, 2003) using a Risø TL-DA-15 reader equipped with an EMI9235QA photomultiplier (Bøtter-Jensen et al., 2000). The feldspar contamination was checked using the IR stimulation (Choi et al., 2009). Only the aliquots that passed the recycling (Roberts, 2006) and recovery (Murray and Wintle, 2003) tests were considered for ED evaluation. All procedures were performed in dim red light. Dose rate measurements were obtained from high-resolution gamma spectrometry measurements (HPGe). Ages were derived from the ratio between ED and dose rate.

4. Results

The Raiale River crosses the PAG fault trace orthogonally, and its set of subparallel splays. It hydrologically connects the Assergi (1000–900 m a.s.l.) and the Paganica Basins (~600 m a.s.l.) flowing through the Camarda (800–700 m a.s.l.) Basin on its footwall (Fig. 2). Owing to the location of the Camarda area location respect to the main PAG fault trace, it offered valuable hints on the Quaternary sedimentation and drainage evolution to constrain the fault activity.

4.1. Geology and stratigraphy

A new 1:10,000-scale geological map was produced (Fig. 3), yielding details on the distribution of the Quaternary continental deposits along the Raiale River. Along with three geological sections (Fig. 4), it illustrates the relationship of these deposits with the main tectonic structures.

The bedrock of the study area is characterized by Jurassic marine formations of the basinal paleogeographic domain, mainly located northwest of the Raiale River, that override the Cretaceous–Tertiary ones of the shelf slope/margin paleogeographic domain through two high-angle, SW–NE-trending faults, with transpressive and kinematics, outcropping close to the Camarda village (Fig. 3). In addition to that, in the area, extensional structures dominate. Some record pre-Quaternary displacement of ~200–300 m, with no evident morphological offset, whereas others, such as the CAM Fault, are well-expressed in the morphology and control the Quaternary continental deposition. In particular, as part of the two main normal fault systems, the total fault displacements are accommodated by the E–W-trending Cesarano (CES; ~80 m) and Assergi (ASF; ~1000 m from Pizzi et al., 2002) Faults; the NW–SE-trending Filetto (FIL; ~230 m) and Paganica Faults (PAG; ~650 m, from Villani et al., 2017) (Figs. 3 and 4). These faults appear to control the northern boundary of the main continental basins of the area, which are, from NE to SW, the Assergi, the Camarda, and the Paganica Basins.

4.1.1. Continental deposits

The Paganica Basin is characterized by the aggradation of the large Middle Pleistocene–Holocene alluvial fan at the Raiale River outlet. Along its eastern edge, it is characterized by a narrow staircase of Early–Middle Pleistocene to Late Pleistocene alluvial terraces (units ALP, SMA, and VIC Fms., Fig. 3), covering a matrix-supported Plio–Pleistocene breccia (MEB Fm., Fig. 3). These alluvial terraces are displaced by the activity of the PAG fault splays, which also dissect the alluvial fan apexes.

The Assergi Basin is mantled by coalescent Middle–Late Pleistocene alluvial fan deposits (AFD in Fig. 3) comprising planar to cross-stratified silt, sand, and conglomerates, dipping southwest, with sediment derived from the dismantling of the Gran Sasso southern slope at the ASF footwall.

The Camarda area presents continental deposits exposed by the Raiale River incision and is located in an open syncline structure (cross section BB', Fig. 4). The continental sequence comprises five confined bodies of clayey silt and breccias represented by the lacustrine deposit (LAC),the slope/cataclastic Vignale Breccia deposit (VGB), the exotic clast-bearing Camarda Breccia (CAB), and the proximal alluvial Cesarano (CEB) and Piana di Cesarano (PCB) Breccia deposits (Fig. 5) (see A1 in Supplementary Materials). This depositional sequence results from a low energy through to a proximal, high-energy, depositional environment unrelated to the present-day Raiale fluvial system. From the stratigraphic relationships of the LAC, CAB, and VGB, as well as the large back tilt (>40°) of the lacustrine layers, it is inferred that the Camarda

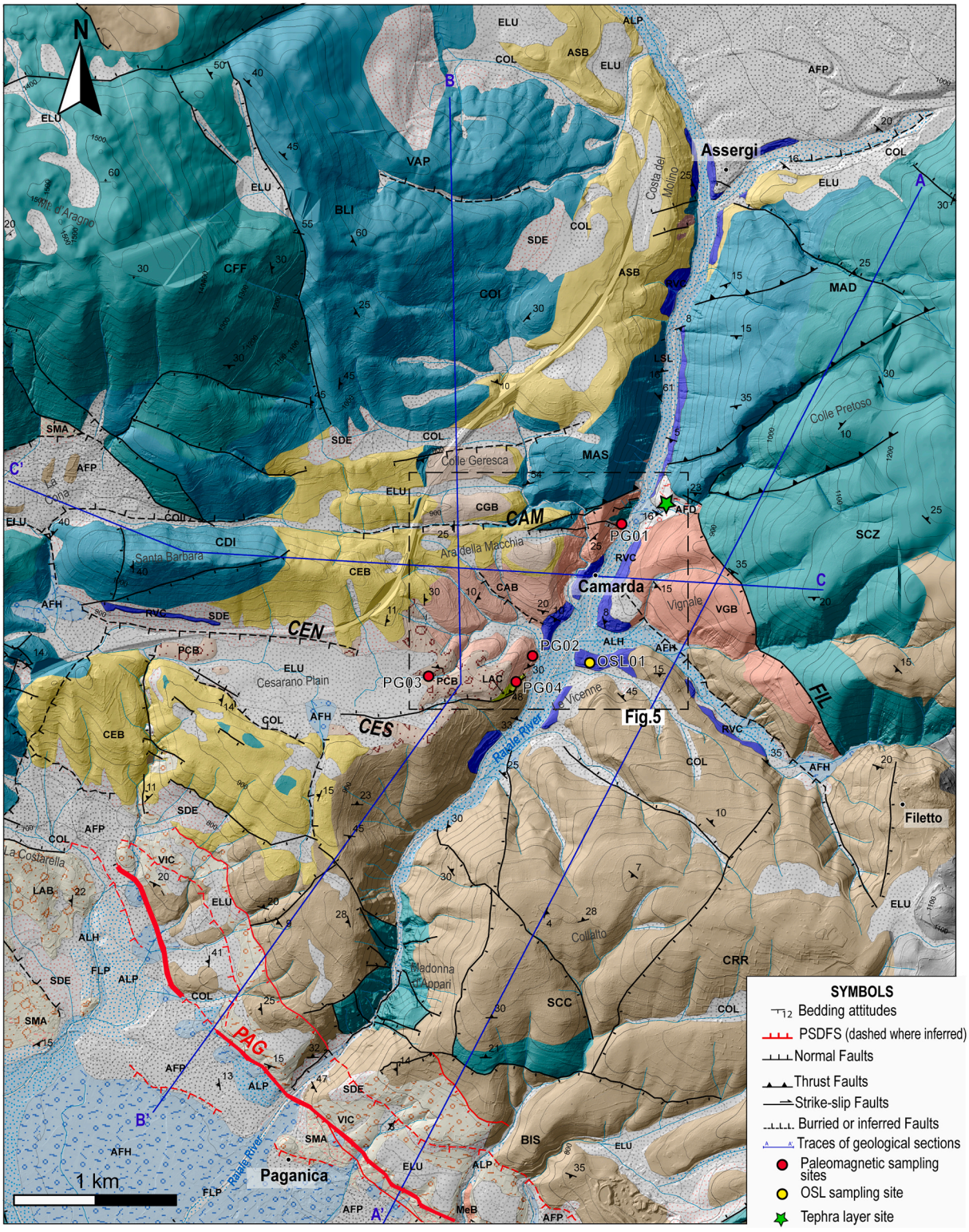

(caption on next page)

Fig. 3. Detailed Quaternary geological map of the Raiale River Basin (Fig. 2). Substratum from Carta Geologica d'Italia, scale 1:50,000 Sheet 359 L'Aquila, ISPRA: Jurassic limestones are Calcare Massiccio (MAS), Corniola (COI), Verde Ammonitico (VAP), and Calcari Diasprigni Detritici Formations; Cretaceous limestones are Maiolica (MAD), Calcareniti e Calciruditi a Fucoidi (CFF), and Scaglia Detritica (SCZ) Formations; and Paleogene–Neogene limestones are Scaglia Cinerea (SCC), Bisciaro (BIS), and Marne con Cerrogna (CRR) Formations. 1-m resolution shaded DTM from Lidar (Civico et al., 2015). Blue traces indicate geological cross sections of Fig. 4. Red circles are the sampling sites of paleomagnetic dating, and yellow circles indicate the OSL sampling site (Section 3.3). (For interpretation of the references to colour in this figure legend, the reader is referred to the web version of this article.)

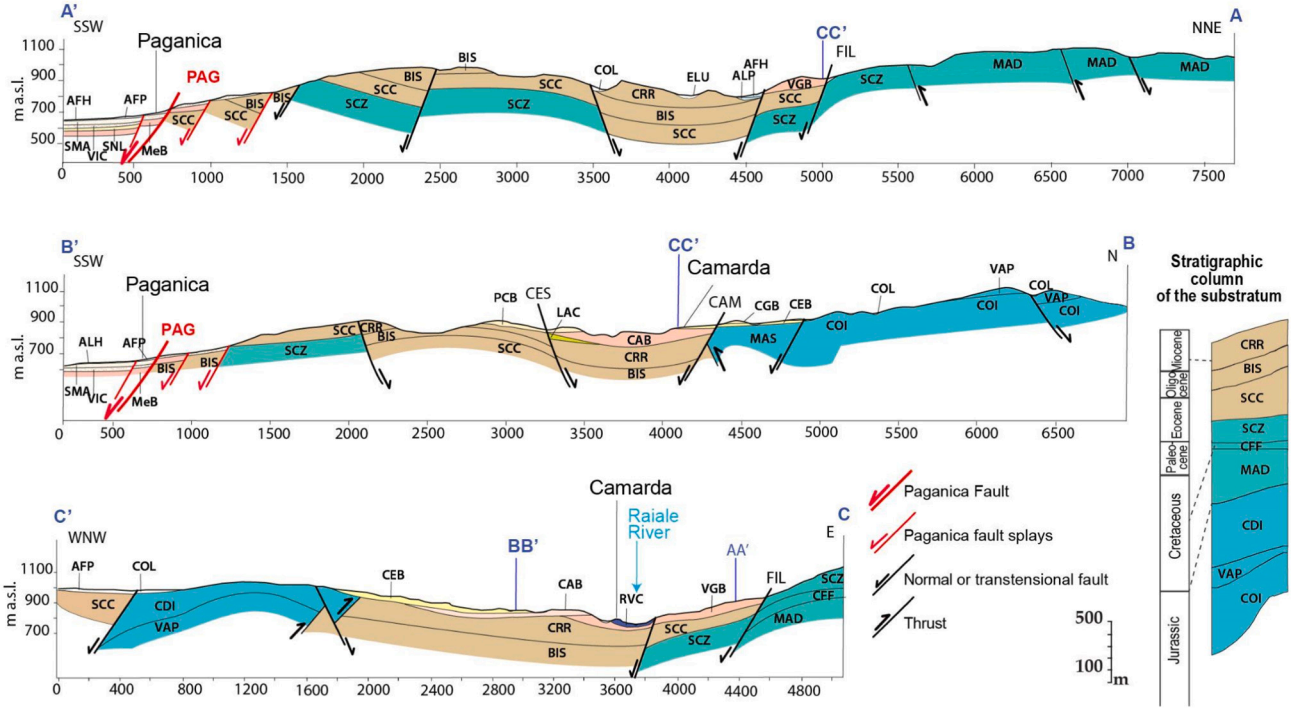

Fig. 4. Geological cross sections orthogonal to the PAG fault splays (in red) and the main compressional structures (AA' and BB') and parallel to the Camarda Basin axis (CC'). See Fig. 3 for the location of the cross section traces. Plio–Quaternary deposits are labeled (COL, AFP, ALF, VIC, SMA, LAC, PCB, CAB, CEB, CGB, VGB, and RVC) and described both in Fig. 3 and in the main text. (For interpretation of the references to colour in this figure legend, the reader is referred to the web version of this article.)

Basin is a syntectonic depression controlled by the E- and NNW-trending CES, CEN, CAM, and FIL faults (Figs. 3 and 5c).

The paleomagnetic sampling has been conducted on the LAC, CAB, VGB, and PCB deposits to support the reconstruction of the Camarda Basin stratigraphy (Fig. 5; see Table A2 and Fig. S2 in Supplementary Material A2 for details). In particular, the LAC and VGB deposits (samples PG04 and PG01, respectively) yield a normal magnetic polarity (Fig. 5a). The CAB deposit (deposited after the LAC) shows a reverse magnetic polarity (PG02 sample in Fig. 5a and b). Finally, the sequence is closed by the PGB deposit (Figs. 5b and c), which records a normal magnetic polarity (PG03).

The normal polarity of the lower members (LAC and VGB) might indicate a Pliocene age of deposition (Gauss normal polarity chron), in agreement with the micropaleontological record of the San Nicandro lacustrine deposits of the Paganica-San Demetrio Basin (Spadi et al., 2016). The magnetic reversal observed for the CABdeposit might suggest an Early Pleistocene age (Matuyama reversed polarity chron), whereas the normal polarity recorded in the upper part of the sequence (PCB) suggests a Middle Pleistocene age (Brunhes normal magnetic chron). Magnetic polarities and stratigraphic relationships chronologically constrain the Camarda Basin to the Pliocene–Early Pleistocene. We do not rule out a possible coeval Late Pliocene onset of the lacustrine deposition (LAC) with that of the MAV Basin (SNL Fm.) (Giaccio et al., 2012; Spadi et al., 2016; Pucci et al., 2019).

Fluvial–alluvial deposits along the Raiale River valley are restricted along its incised channel. The oldest is the Ancient Fan Deposit (AFD, Fig. 5), a unit positioned up to 90 m above the present-day river talweg, northeast of Camarda village. It contains an extensive and well-preserved 40-cm-thick brown paleosol topped by a ~10-cm-thick reworked tephra layer (green star for location in Figs. 3 and 5), which can be roughly correlated to those found elsewhere in the L'Aquila area. In particular, tephra and volcanoclastic material were found in several sites close to the Paganica area and these were dated to between 365 and 460 ka (correlated to the well-known eruptions of the Latium volcanic districts; Giaccio et al., 2012). Despite the tephra being reworked, it can be reasonably assumed that it is not older than 460 ka. The terraced fluvial–alluvial deposits that are disconnected from the present-day Raiale River dynamics comprise the Raiale Valley Conglomerates (RVC; Figs. 3 and 5). They comprise clast-supported conglomerates composed of cross-stratified and imbricated coarse gravels, mainly from the carbonate Meso–Cenozoic sequence. The RVC presents laterally continuous and well-defined subhorizontal treads, locally well-cemented, and erosional bases on bedrock or Quaternary sediments.

4.2. Geomorphology

4.2.1. Morphostratigraphy and Quaternary evolution

The vertical/lateral relationships among the clastic formations of the Camarda Basin described in Section 4.1.1 are associated with depositional and erosional surfaces. Relative and absolute chronologies, altitudinal range, and morphological cross-cutting relationships between tectonic landforms and paleosurfaces were used to reconstruct the main phases of the morphotectonic evolution of the study area.

The confinement of the E–W elongated Camarda Basin suggests a

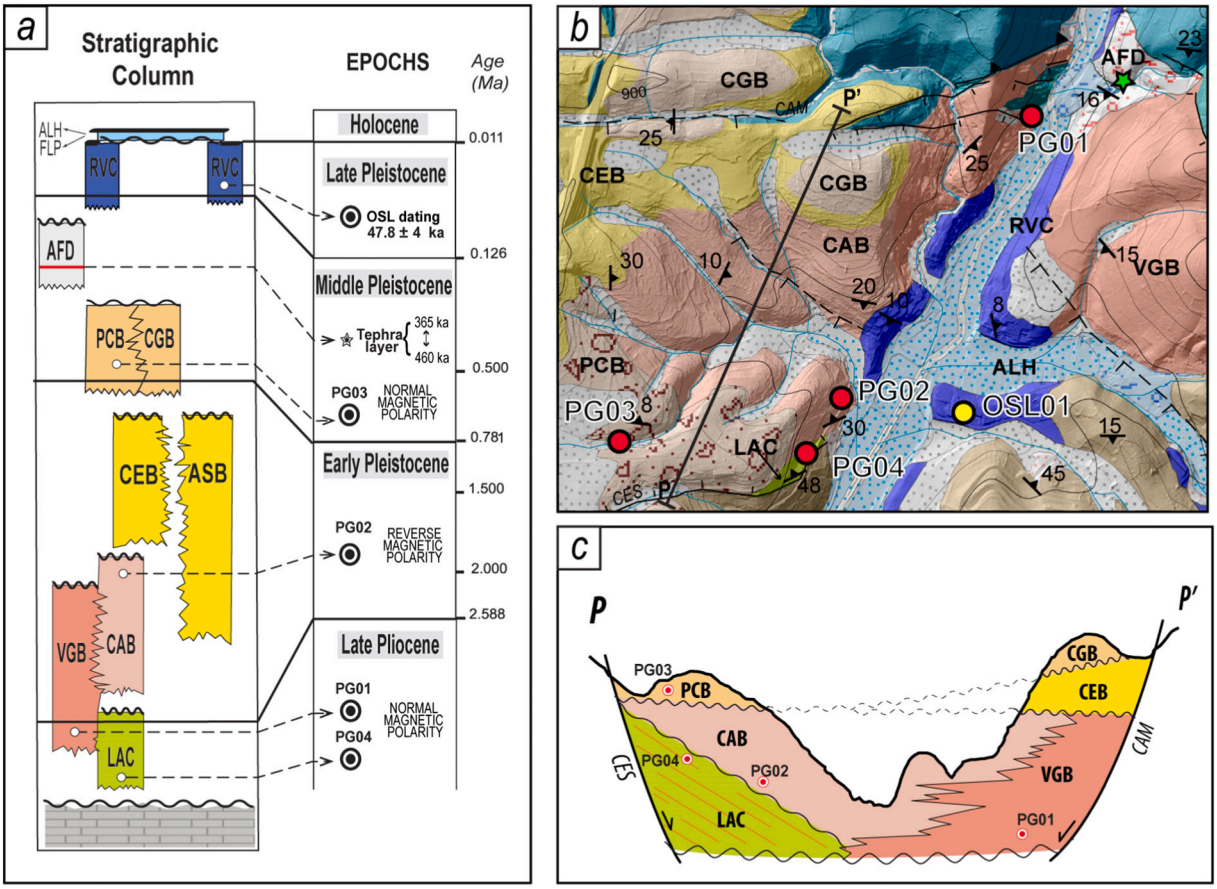

Fig. 5. (a) Stratigraphic column of the Quaternary deposits in the study area (modified after Pucci et al., 2019); From older to younger deposits there are lacustrine deposits (LAC), Vignale Breccia (VGB), Camarda Breccia (CAB), Cesarano Breccia (CEB), Assergi Breccia (ASB), Piana di Cesarano Breccia (PCFB), Colle Geresca Breccia (CGB), Raiale Valley Conglomerates (RVC), Alluvial Holocene Deposit (ALH), and Fluvial Pleistocene Deposit (FLP). In the panel, the paleomagnetic and OSL dating are indicated, along with the reworked tephra found within the AFD deposit and possibly correlated with those from Giaccio et al. (2012). (b) Geological map of the Camarda Basin (location in Fig. 3) with the attitude of the depositional bodies and sampling locations indicated. (c) Schematic geological section PP' (location in panel b) shows different interfingering of depositional bodies.

possible initial hydrological disconnection from the proto-MAV Basin, as hypothesized for similar basins by Geurts et al. (2020). Its infilling, comprising the LAC, CAB, and VGB deposits, is topped by a paleosurface, positioned at ~950 m a.s.l. and related to the ancient phases of relief smoothing, associated with the deposition of CEB and the ASB Breccia deposits. (Figs. 6 and 7). This gently rolling landscape (hereafter termed the Cesarano paleosurface) runs along the Raiale River's right-hand side and is inset in the high-standing low-relief surface carved on the Meso–Cenozoic substratum of Mt. d'Aragno. This paleolandscape resembles a NE–SW-elongated paleovalley, suggesting the occurrence of a proto-Raiale valley positioned at higher elevations (from ~175 to 205 m) above the present-day Raiale River talweg (Figs. 3 and 6). The Cesarano paleosurface correlates with the erosional surface of Collalto (~975 m a.s.l.) on the Raiale River's left-hand side (Fig. 6). A depositional surface of the PCB and CGB deposits unconformably lies at an elevation of 875 m a.s.l (hereafter termed the Cesarano plain), possibly displaced by E-trending normal faults.

Such landscapes are deeply incised by the Raiale River, which cuts a deep gorge connecting the Assergi Basin to the Paganica-San Demetrio Basin (Figs. 6 and 7). At the Raiale River outlet a large Holocene alluvial fan developed within the dissected Early–Middle Pleistocene terraces.

4.2.2. *Present-day Raiale River longitudinal profile*

The present-day Raiale River, mainly fed by discharge from the Gran Sasso Range, is ~17 km long and has a catchment of 106 km^2 with an asymmetric shape. Its path is almost rectilinear and shows an abrupt flow direction change from ESE, in the Assergi Basin, to SSW from the Assergi Village, crossing the PAG (Fig. 8a).

The longitudinal profile of its main stem is characterized by three different sections separated by two knickzones: the upstream concave-up profile (up to 4000 m downstream distance) with a K_{sn} of 85.4 (see Supplementary Material A4 for major details); the intermediate section that shows a slight concave-up profile has a K_{sn} of 85.9) (between the Assergi and Paganica Basins); the concave lower reach (from just upstream the PAG Fault to the local base level of the Paganica-San Demetrio Basin) shows a K_{sn} of 100 (Fig. 8b).

Consequently, a first knickzone (K1) is located upstream of the Assergi Basin, ~10 km from the PAG Fault and shows a convex profile at a downstream distance between 4000 and 6000 m (Fig. 8b). A second knickzone (K2) is located downstream, ~1500 m, before the PAG fault trace, where the longitudinal profile slightly increases in slope, showing a convexity between 13,000 and 14,000 m (Fig. 8b).

The Raiale River main stem in the PAG footwall mainly shows a bedrock talweg, dominated by detachment-limited (sensu Tucker and Whipple, 2002) erosional processes and associated with V-shaped cross-valley profiles (Fig. 8c). The bedrock talweg is composed of marly limestones (SCC-CRR Fms.) and limestones (COI-SCZ Fms.) with slightly different erodibility that does not control the knickzones (Fig. 8b). When the talweg passes over thin alluvial deposits of the Assergi and Camarda Basins, the cross-valley profiles widen and flatten (profiles b and d, Fig. 8c). In the proximity of the PAG footwall knickzone K2, a deep gorge develops in bedrock, with valley-side cliffs (up to ~100 m high) and

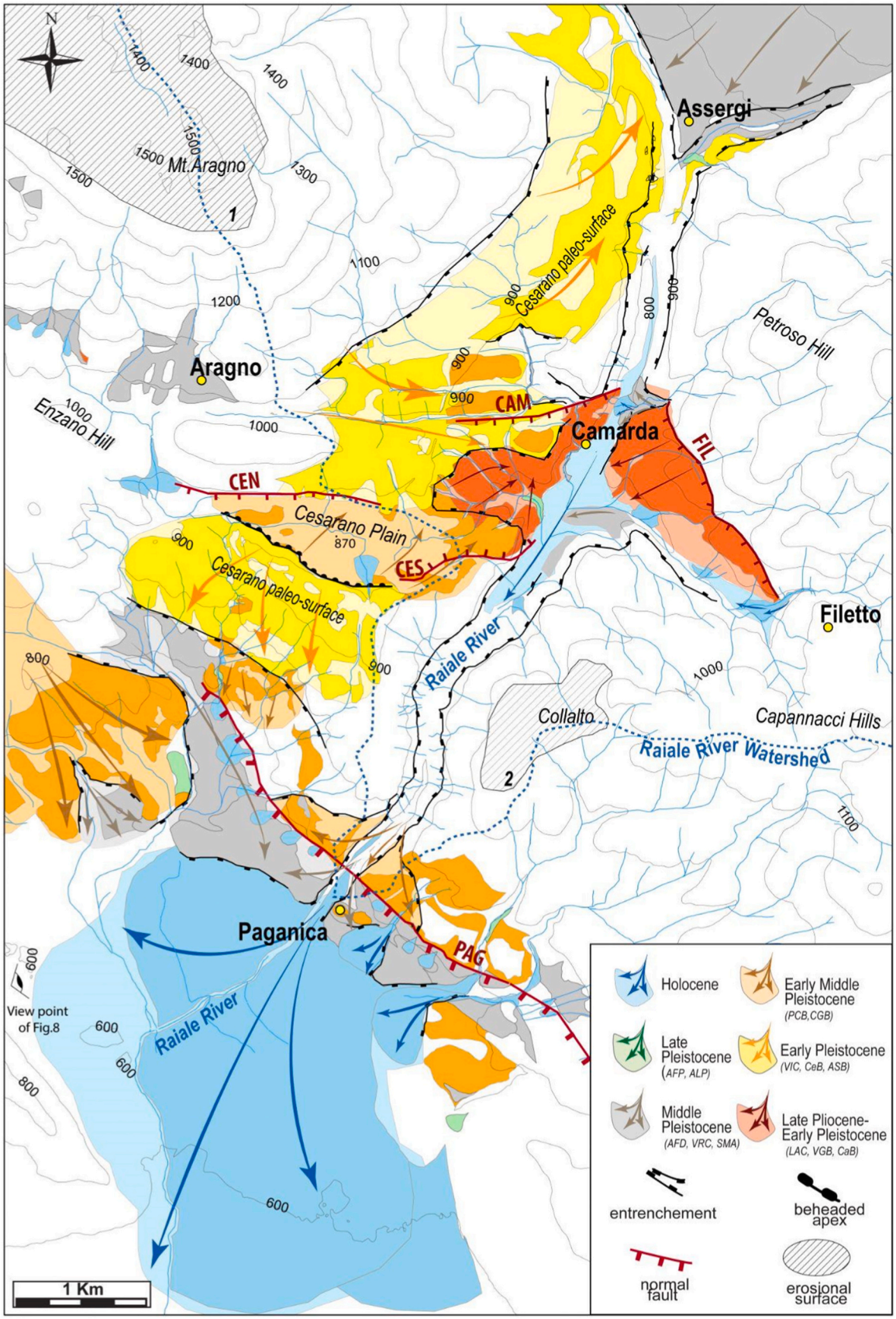

Fig. 6. Scheme of the cross-cutting relationships between the continental sediment bodies in the footwall of the Paganica Fault. Light-colored polygons represent the hypothetical original depositional body extent. Dark-colored polygons are the depositional bodies outcropping in the field, and arrows indicate the main inferred paleoflow directions. The Paganica, Filetto, and Cesarano normal faults, the main body entrenchments, and the beheaded apexes are reported (modified from Pucci et al., 2019). Erosional surfaces are indicated.

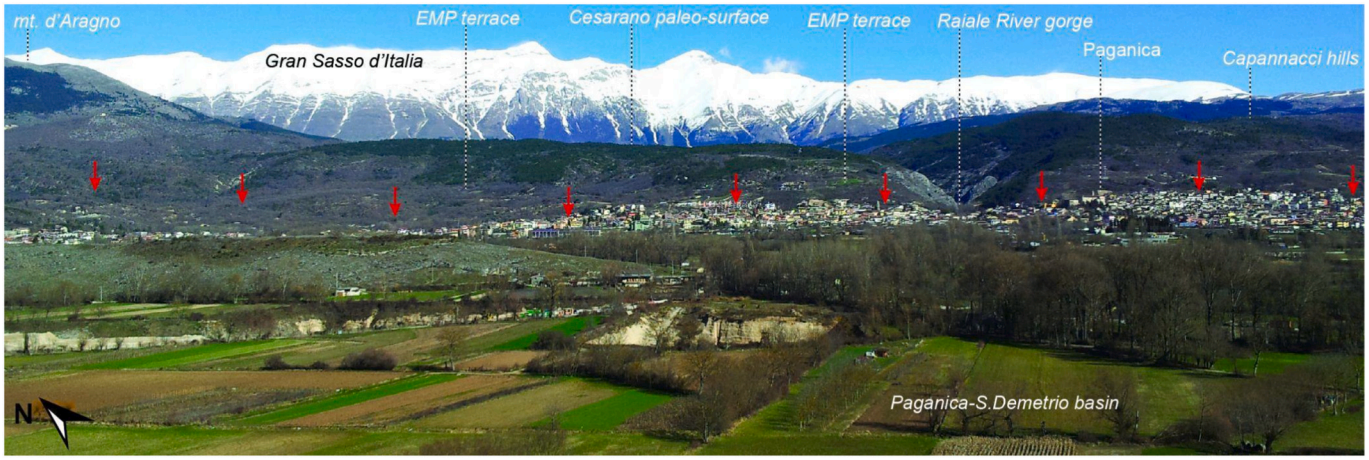

Fig. 7. View of the Raiale River outlet and the Paganica-S.Demetrio Basin, where its Holocene alluvial fan develops (viewpoint in Fig. 2). Red arrows point to the main PAG surface trace affecting the Early–Middle Pleistocene terraces (EMP). The gorge notably incises the hanging upper Cesarano paleosurface (image foreground). In the background, the Gran Sasso Range watershed of the Raiale River is visible. (For interpretation of the references to colour in this figure legend, the reader is referred to the web version of this article.)

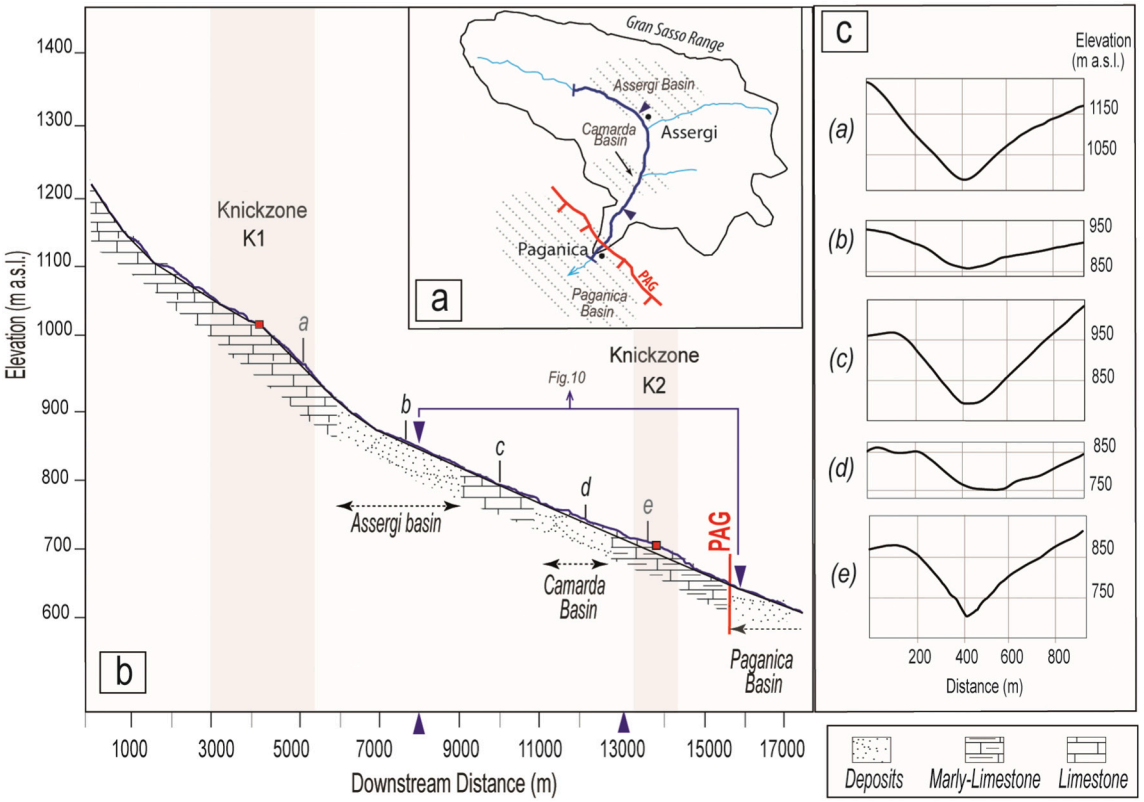

Fig. 8. (a) Sketch of the Raiale River Watershed and the main drainage lines crossing the three basins of Assergi, Camarda, and Paganica; (b) longitudinal profile of the Raiale River main trunk (dark blue in panel a). The two principal knickzones, K1 and K2, and the talweg type (bedrock vs. alluvial deposits) are indicated. Vertical exaggeration is 2×; (c) cross-valley profiles (see location in panel b). Vertical exaggeration is 2×.(For interpretation of the references to colour in this figure legend, the reader is referred to the web version of this article.)

very narrow bedrock valley floor, suggesting significant rejuvenation by fluvial incision (profile e, Fig. 8c).

4.2.3. *Fluvial terraces along the Raiale River valley*

Along the Raiale River valley, between the Assergi and Paganica Basins, flights of fluvial terraces were recognized and mapped (Supplementary Material A3). Over 60 terrace treads were identified and outlined by both inner and outer edges. Apart from a few cases, most of the fluvial terraces (composed of RVC., Fig. 3) are unpaired and show a strath-terrace nature, being very thin (<3–4 m). They lie a few meters (~5 m) above the present-day talweg in the Assergi Basin while reaching up to 80 m immediately north of the Paganica Basin. Owing to the limited thickness and clear-cut top of the deposits, the elevation difference was considered between the treads of the fluvial terraces flights as a reliable expression of the elevation change instead of that calculated from their erosional base (i.e., strath).

In the Camarda area, terraces tend to be more preserved with broad surfaces than those along the valley because of a tributary from the left side (Fig. 6). In fact, along the steep V-shaped valley flanks, hillslope processes dominate, and terraces are likely to be less maintained (Fig. 8). Here, fluvial deposits comprise small, terraced remnants with scarce to poorly preserved margins because of slope processes that erode the outer risers or cover the inner edges with colluvial wedges.

Based on their continuity, average elevation range, and talweg-related elevations (i.e., topographic difference with the present-day Raiale River as baseline), the correlation of five terrace levels were possible using linear regression (Fig. 9). In particular, if the population of terraces at distances of 8000–9000 m is considered, the talweg-related elevations for each terrace level are as follows: level I, 38.5 ± 11 m; level III, 21.3 ± 3 m; level IV, 10.9 ± 3 m; and level V, 3.5 ± 1 m. The same terrace levels at downstream distances of 11,500–12,500 m have the following elevation: 66.9 ± 10 m for the level I; 35.5 ± 1 m for level III; 25.9 ± 3 m for level IV; and 13.1 ± 7 m for level V, the youngest terraces. The Level II terraces, having a limited extent through the Raiale River Valley, are found from 9500 to 11,300 m with elevations above the modern talweg from 22.7 ± 1 to 31.1 ± 3 m. Hence, the talweg-related elevations of each terrace level increase downstream. This evidence denotes a positive gradient in the incision rate approaching the PAG Fault.

4.3. Incision and erosion rate estimate

The five levels of fluvial terraces recognized along the upper reach of the Raiale River were crucial to estimating incision rates, which were subsequently compared to denudation rates obtained for the low-relief uplands of the drainage basin.

4.3.1. Paleolongitudinal profile age and incision rates

At an elevation of 12 m from the talweg, terrace level V close to Camarda village was sampled (distance 11,300 m, Fig. 9), where the terrace is well-preserved and continuous with a thickness of ~10 m. The OSL analysis provided an age of 47.8 ± 4 ka for the terrace level V (Table 1). Considering its talweg-related elevation, an incision rate of 0.25 ± 0.02 mm/a for the youngest paleolongitudinal profile of the Raiale River at the sampling point was determined.

Assuming a relatively constant incision rate of 0.25 ± 0.02 mm/a over the Pleistocene, the possible age range of the terrace flights from their talweg-related elevation at the sampling point can be inferred (Fig. 10). Afterward, their possible match with favorable climatic stages was checked by correlation with the OIS curve (Lisiecki and Raymo, 2005) considering that their worldwide cyclic formations might have been a response to climatic fluctuations (Bridgland and Westaway, 2008). Starting from the dating age of the terrace level V tread, whose

Table 1
Results of the OSL analysis. All errors are at one sigma except for ED (two sigma). See Figs. 3 and 4 for locations.

OSL ID	Lab	Grain size Ø (μm)	ED (Gy)	DR (mGy/h)	Age (ka)
CAM1	Ph3dra-INFN	180–212	70.8 ± 5.8	1.48 ± 0.3	47.8 ± 4.0

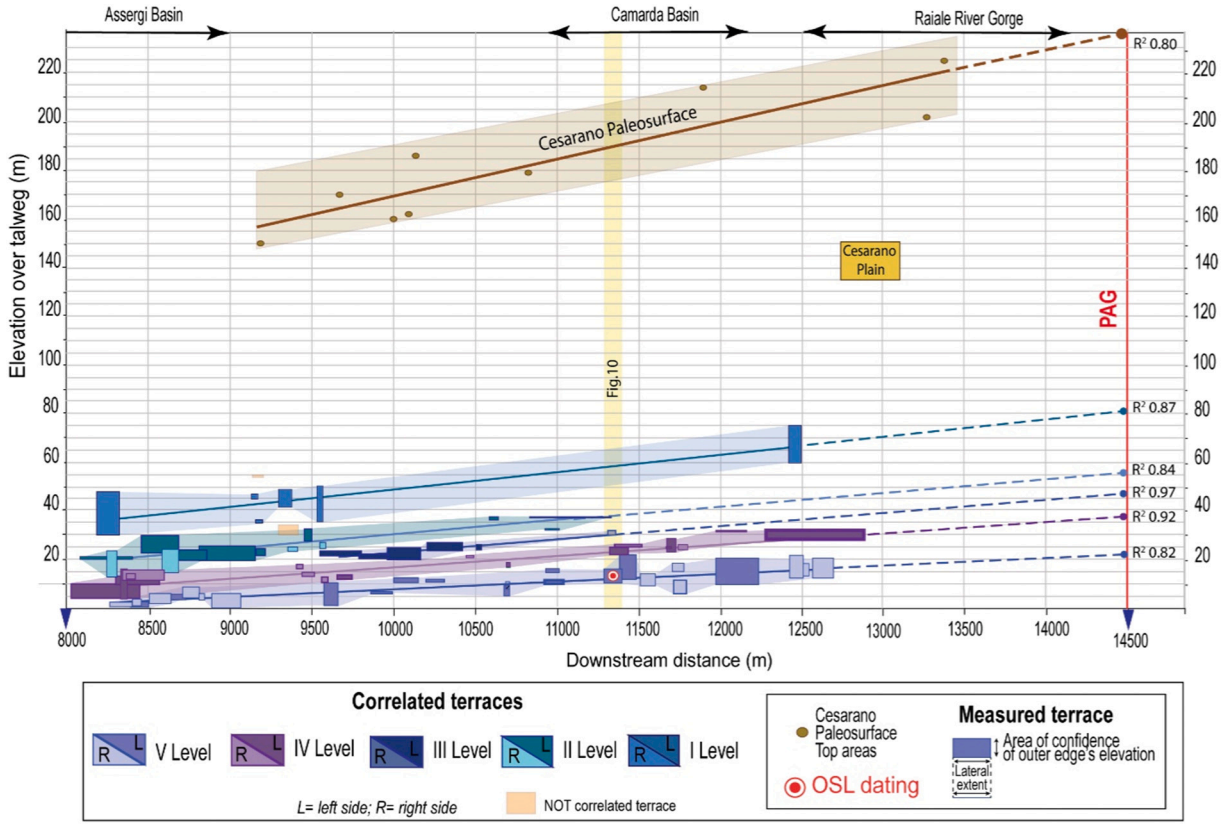

Fig. 9. Projected longitudinal profiles of the elevations of river terraces along the two sides of the Raiale River present-day talweg (see Fig. 9a for the baseline location). The solid boxes describe the elevation range of the outer edges. The box width accounts for the lateral extent of each detected terrace. The box height points to the elevation uncertainty (measured at the beginning and end of each terrace edge). The correlation (linear regression line) of the average elevation for each terrace level is reported as a solid line and its projection on the PAG fault is reported as a dashed line. The correlation coefficient of each level of terraces is also indicated. All the elevations are relative to the zeroed talweg. Elevation points measured at the top areas of the Cesarano Paleosurface and elevation of the Cesarano plain are also reported. Light-colored areas indicate the range of elevation of each dataset group (i.e., terrace level and paleosurface).

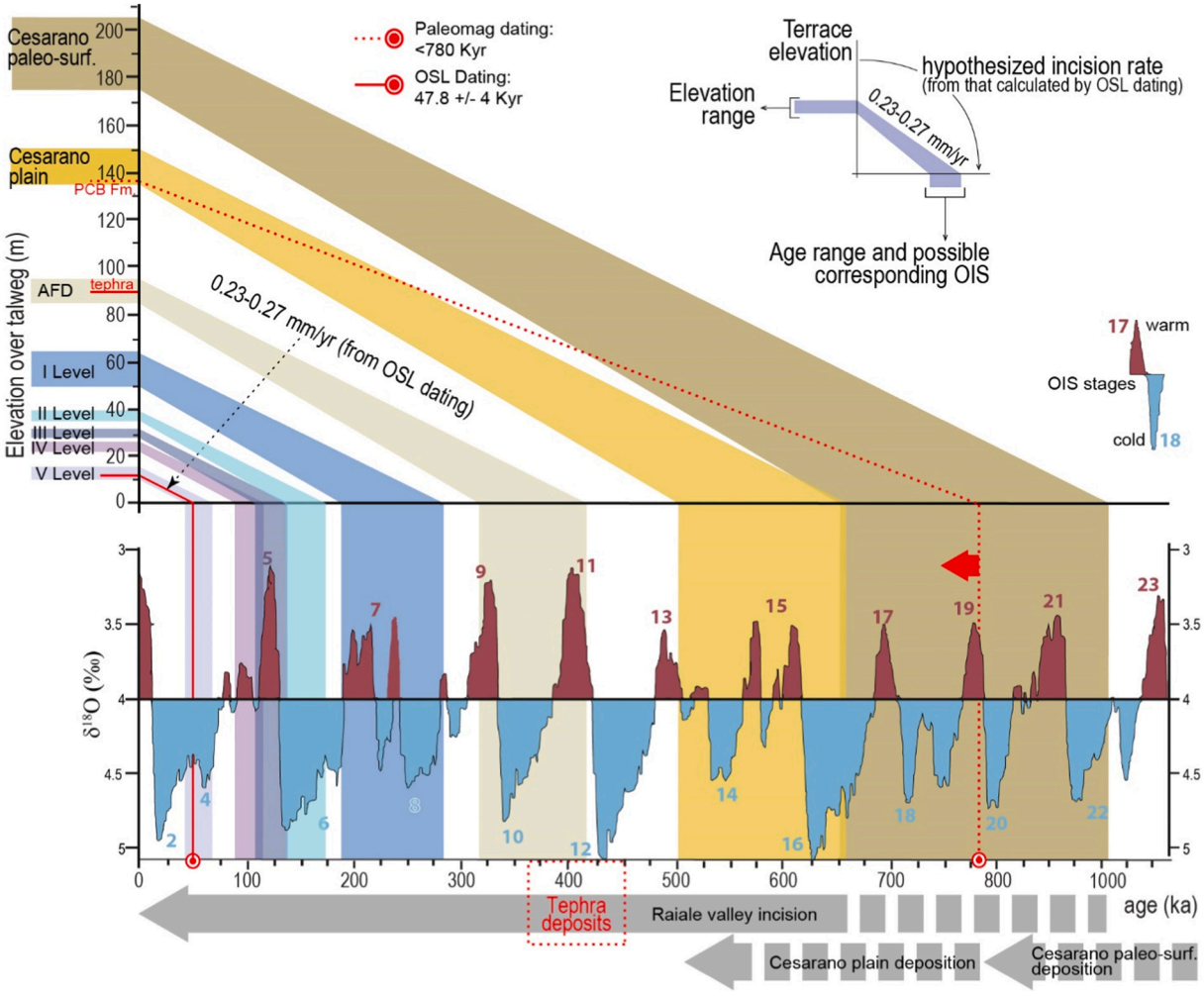

Fig. 10. Correlation of the Raiale River terrace distribution and Cesarano paleosurface with the OIS time curve of Lisiecki and Raymo (2005). The incision rate estimated from the OSL dating of terrace level V is reported and applied for correlating the river terrace levels and paleosurface elevation with the isotopic time curve. The correlation applies to the OSL sampling point (see Fig. 9 for the location along with the Raiale River longitudinal profile).

deposition occurred at the OIS 3/4, the sequence of the terrace levels IV, III, II, and I can tentatively be correlated with OIS 5c/d, 5d/6, 6, and 8, respectively. The evidence that the obtained ages of these fluvial terraces fit well the aggradation processes that occurred during glacial periods further supports our hypothesis of a fairly constant incision rate through time. The fluvial terraces appear to be preserved starting from 300 ka ago.

The same incision rate of 0.25 ± 0.02 mm/a assigned to the Ancient Fan Deposit (AFD, Fig. 3), which contains the reworked thick tephra layer and is positioned up to 90 m above the nearby present-day river talweg, matches quite well the period of tephra deposition that occurred in the area before 460 ka ago (Fig. 10).

Similarly, if a constant incision rate of 0.25 ± 0.02 mm/a is assumed since the onset of the Raiale River all along the main stem, an age for both the Cesarano paleosurface and the Cesarano plain dissections can be inferred. The Cesarano plain stands at ~135–150 m above the talweg (Fig. 9), and its estimated incision onset is in the range of 500–655 ka. This age agrees with the upper age limit of 780 ka, constrained by the magnetic polarity of the PCB deposit forming the reference plain (Fig. 10). Meanwhile, the Cesarano paleosurface stands at ~175–205 m above the talweg, and the inception age of its downcutting could be 0.65–1.0 Ma (Fig. 10).

4.3.2. *Denudation rates from terrestrial cosmogenic nuclides (TCN)*

For the denudation rates estimation of the summit using ^{36}Cl sampling of the low-relief uplands (1200–1550 m a.s.l.) in the vicinity of the Raiale River's watershed was conducted (Fig. 2). The RA-E02, RA-E03, and RA-E01 samples were collected from Cretaceous limestones. Sampling locations were from the top of Mt. d'Aragno, at the eastern-most side of the Raiale watershed and on the divide between the Stabiata and the Collebrincioni Basins. In addition, the RA-E04 sample was collected from Jurassic limestones on the Capannacci Hills.

From the 3-cm-thick rock samples (density of 2.7 g/cm^3), the ^{36}Cl concentrations were determined. The number of neutrons and muons found in each sample and the related grams of Ca/CaO in the processed rock sample are shown in Table 2. The measured ^{36}Cl amount ranges

Table 3
Sample location and the amount of calcium in the samples. See the main text for a description.

Name	Long	Lat	Altitude (m)	mCa/m rock dissolved [g/g]	CaO [%]
RA-E01	13.4152	42.4080	1283	0.23 ± 0.002	32.2
RA-E02	13.4594	42.4105	1548	0.393 ± 0.004	55.1
RA-E03	13.5466	42.3904	1448	0.463 ± 0.003	64.8
RA-E04	13.5234	42.3612	1206	0.398 ± 0.003	55.6

from 1.37 × 10^8 to 2.22 × 10^8 atoms (Table 3), three orders of magnitude higher than that measured in the blanks (1.52 × 10^5 atoms of ^{36}Cl). The measured amount of natural chlorine ($Cl-_{nat}$) in the samples is 2–3 orders of magnitude higher than that of blank: it ranges between 2.6 × 10^{20} and 6.6 × 10^{19} atoms versus the 2 × 10^{17} atoms in the blank. Using the Schimmelpfennig et al. (2009) spreadsheet and corrections for altitude and latitude from Stone (2000), the denudation rates of the samples were determined (Table 3).

The values clustered around 24–44 m/ka. The lowest value is from the RA-E02 sample located at the highest elevation, while the others give similar results. The mean denudation rate at the footwall of the Paganica normal fault, calculated from TCNs, is 0.02–0.04 mm/a.

4.4. Plio–Pleistocene evolution of the area

By integrating the stratigraphic, morphotectonic, and paleomagnetic data, a Quaternary evolution model of the studied area was proposed, composed of four different stages that led to the emplacement and development of the Raiale River in its current form.

(1) Late Pliocene–Early Pleistocene. In the Late Pliocene, the development of E–W- and NNW–SSE-trending fault systems occurred, in agreement with the evolution model proposed for the MAV by Pucci et al. (2019). These fault systems led to the genesis of the Camarda tectonic satellite Basin, E–W elongated and narrow, isolated by structural bedrock highs. The Camarda depositional sequence unconformably lying on the Meso–Cenozoic substratum is composed of an early lacustrine deposition (LAC), followed by confined bodies of breccia (VGB and CAB) that progressively infilling the basin (Fig. 11 a-b). Notably, in the study area, based on the normal polarity of paleomagnetic data, the lacustrine deposition occurred starting from the Pliocene. This appears to be coeval with the Late Pliocene onset of the lacustrine depositions of the San Nicandro Fm. in the MAV Basin (Spadi et al., 2016; Pucci et al., 2019). After increasing the *syn*-rift topographic relief, an Early Pleistocene environmental change led to high-energy deposit production and slope debris/breccia deposition in dry or transport-limited conditions. The evidence of numerous syntectonic depositions denotes a long-lasting activity of the basin-bounding E–W-trending normal faults.

This initial phase predates the Raiale River gorge's incision, as testified by the breccias paleoflow and bedding dip directions converging to an E–W oriented depocenter, which is now disjointed from the present-day morphodynamics.

(2) Early Pleistocene. A depositional phase of breccia deposits (CEB/ASB) showing reverse paleomagnetic polarity, has filled to the brim the Camarda Basin and has covered with a marked angular unconformity the shallow-dipping CAB and VGB. The deposition drapes a wide NE–SW-trending paleovalley, inset between Mt. d'Aragno and Capannacci Hills, forming the early connection between the Assergi and the Paganica Basins (Fig. 11c). Its geometry suggests a landscape influenced by the paleodrainage activity of the proto-Raiale River. The deposition's lack of distal alluvial facies is possibly due to the immature drainage catchment and prevalent supply from high-gradient slopes. The present-day gentle NE-sloping of the paleovalley can be related to the post-Early Pleistocene footwall back-tilting due to the intervening PAG activity.

(3) Late Early Pleistocene–Middle Pleistocene. Entrenchments locally start to interrupt the lateral continuity of the Cesarano land surface (Fig. 11d). Limited breccia bodies (PCB and CGB) prograde toward the paleo-Raiale River and infill inset E–W-elongated, fault-controlled narrow basins. It can be inferred that the Cesarano plain formation occurred at ~500–650 ka from the estimated constant incision rate.

The limited dissection of the Cesarano paleosurface suggests a reduced activity of the E–W-trending normal faults (e.g., CES, CEN, and SW faults). At the end of this phase, the Raiale River starts to incise the Cesarano paleosurface (Figs. 10 and 11e). This testifies to ongoing PAG activity that progressively lowered the Raiale River base level (i.e., the Paganica-San Demetrio Basin, on the hanging wall), elevating the Cesarano paleosurface up to >200 m above the present-day talweg.

(4) Late Middle Pleistocene–Holocene. The activity of the PAG continues to trigger the headward erosion of the Raiale River drainage and the deepening of the longitudinal profile at its footwall. Concurrently, stadial and interstadial phases drive the formation of a set of fluvial terrace flights, inset into the Raiale River valley, progressively disconnects from the stream dynamics (Fig. 11f).

The incision record documented for the Raiale River valley suggests its inception during the Late Early Pleistocene-beginning of the Middle Pleistocene (Fig. 10). This is in agreement with (1) the increased activity of the NW–SE-trending normal faults (Pucci et al., 2019) that, according to some authors, is due to the fault linkage acceleration invoked for this sector of the Apennines (Roberts and Michetti, 2004; Whittaker et al., 2007b; Whittaker et al., 2008); (2) the timing of the drainage integration of the Paganica-S.Demetrio Basin into the regional Aterno River system (0.7–0.8 Ma) (Geurts et al., 2020); and (3) reduction in sediment supply at the end of the Mid-Pleistocene climatic transition (0.7–1.25 Ma) (Whittaker et al., 2010; Whittaker and Boulton, 2012; Head and Gibbard, 2015; Willeit et al., 2019).

Table 4
Accelerator mass spectrometry measurements of the $^{35}Cl/^{37}Cl$ ratio, the number of atoms of Cl_{nat} and ^{36}Cl, and the corresponding atoms of ^{36}Cl per gram of rock. The denudation rate (mm/a) is determined with the Excel spreadsheet of Schimmelpfennig et al. (2009). See the main text for a description.

Name	n(^{35}Cl)/n (^{37}Cl)	Atoms Clnat (x 10^{19})	Atoms ^{36}Cl (x 10^8)	Atoms $^{36}Cl_{corr}$/g of rock (x 10^6)	Denudation rate (m/ka)
RA-E01	3.64 ± 0.01	26.1 ± 0.69	2.22 ± 0.08	3.14 ± 0.1	40.8 ± 4
RA-E02	5.07 ± 0.02	6.89 ± 0.10	1.60 ± 0.05	2.07 ± 0.08	23.6 ± 2
RA-E03	5.12 ± 0.02	6.70 ± 0.12	1.46 ± 0.05	1.96 ± 0.07	43.7 ± 4
RA-E04	5.08 ± 0.03	6.93 ± 0.14	1.37 ± 0.05	2.21 ± 0.08	36.1 ± 3

4.5. River incision and long-term slip rate of the Paganica fault footwall

A graded theoretical profile (for details, see A4 in Supplementary Materials) connecting the local base level (i.e., Paganica-San Demetrio Basin) with the upper reach (p3) indicates equilibrium. The Raiale River would tend to this equilibrium if there were no perturbations (Fig. 12). Conversely, the Raiale River longitudinal profile is interrupted and subdivided into different sections by knickzones k1 and k2, denoting an ungraded status. Therefore, the different sections of the present-day Raiale River longitudinal profile (Fig. 8b) can be extrapolated downstream to represent their theoretical equilibrium. The upstream profile (p1) is graded with a concave-up form, and is positioned above the Raiale River talweg up to an elevation of ~250 m approaching the PAG fault (Fig. 12). This configuration mimicks the elevated position of the Late Early Pleistocene Cesarano paleosurface elevation trend (Figs. 5a, 6, and 9). The more rectilinear profile configuration of the intermediate section (p2), which contains river terrace flights, is projected to the

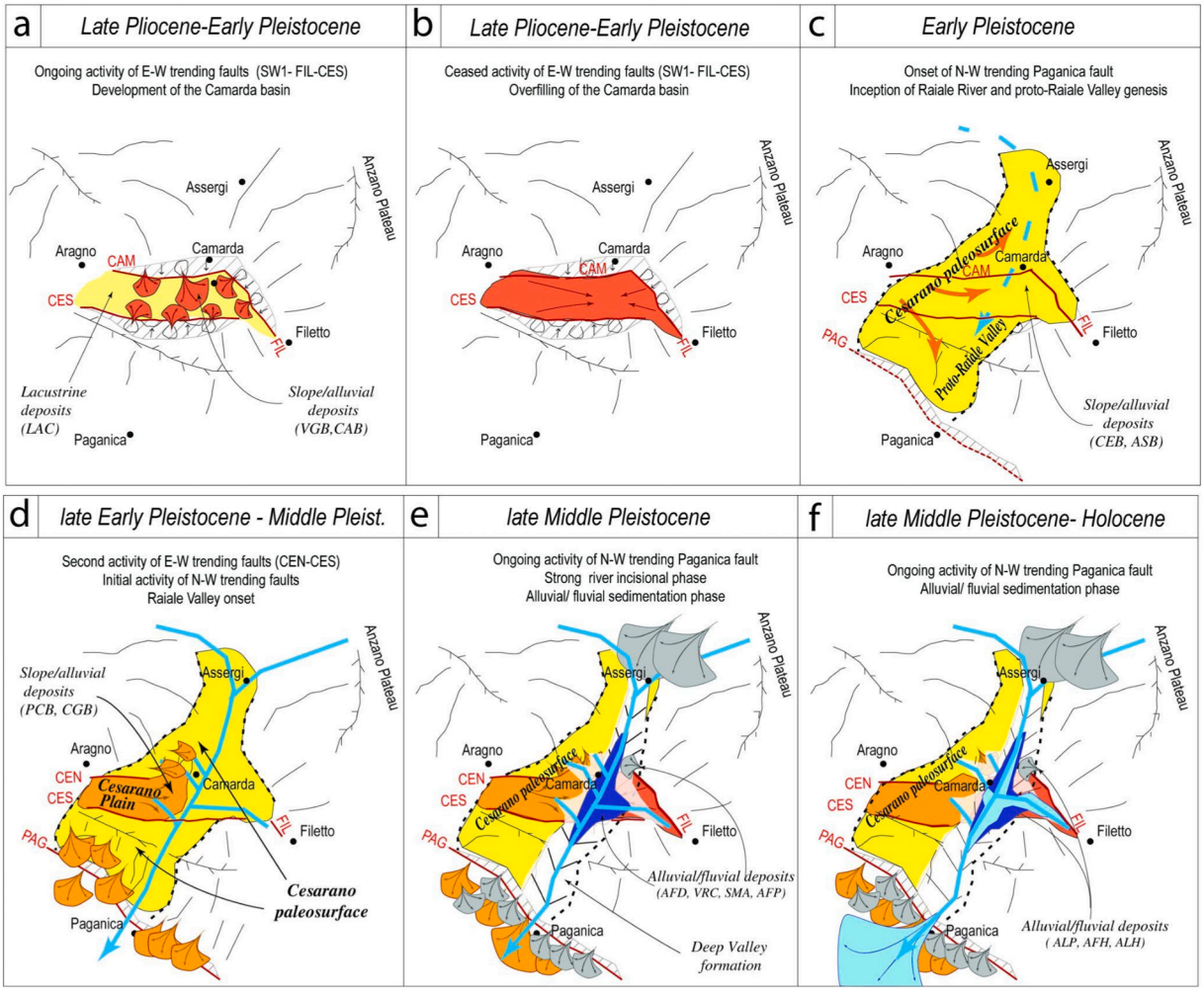

Fig. 11. Sketch of the evolution of the Raiale River studied area from the Late Pliocene to the Holocene. See the main text for details.

Raiale River outlet at an elevation of ~50 m above it.

Assuming these knickzones are not lithologically controlled, they constitute perturbations of the Raiale River profile, which respond to external base-level changes that must be communicated upstream until the whole catchment eventually reaches a new steady state topography. Such knickzones propagate through episodes of transient regressive erosion that adjust the longitudinal river profile (Pazzaglia et al., 1998; Whittaker et al., 2007a, 2007b).

The knickzone k1 appears to mark the upstream extent of the headward propagating incision wave affecting the Cesarano paleosurface. Considering its age of ~1.0 Ma and the ~12-km horizontal distance from PAG, an average migration rate of ~12 mm/a is found, similar to that of Whittaker et al. (2008) in response to active faulting in the Central Apennines. Furthermore, the well-preserved knickzone k1 could represent a transient landform (i.e., *not* in a topographic steady state) probably triggered by new tectonic forcing that commenced prior to the Middle Pleistocene.

Similarly, the knickzone k2 in a more intermediate region of the Raiale River longitudinal profile illustrates the incision wave affecting the p2 section near the PAG fault. The resulting convexity represents a transient landform that indicates a younger perturbation (applying the k1-derived migration rate could have initiated around 125 ka), possibly related to the increase in footwall uplift, the decrease in water discharge (following the last interglacial period), and the lithological control of the Raiale bedrock gorge compared to the Paganica-S. Demetrio Basin.

Certainly, the intermediate sector of the Raiale River longitudinal profile, upstream of k2, presents elevated paleolongitudinal profiles depicted by the five levels of strath terraces (Figs. 9 and 12). These paleolongitudinal profiles diverge downstream. Such a divergence indicates a footwall uplift gradient approaching the PAG Fault, invoking a tectonic control for the present-day longitudinal profile.

In this context, the incision rate of the Raiale River is strictly connected to the capability of the drainage system to respond to changing tectonic uplift and adjusting to the new base-level conditions (i.e., PAG hanging wall subsidence). Considering that a steady-state downcutting of the uplifting footwall is not reached and the Paganica alluvial fan aggradation sustains the concave-up profile (p3) at the subsiding hanging wall, the incision rate of the Raiale River can provide a minimum estimate of the PAG throw rate.

We assume the hypothesis of a constant incision rate along the entire stem, although some authors observed oscillations in the rate that tend to decrease mountainward (e.g., Zhang et al., 2018). Nevertheless, such probable oscillation might be embedded in the uncertainty range of the incision rate estimation. In fact, the evidence that the proposed timing of the Raiale River valley evolution (Fig. 10) agrees with the stratigraphic framework reconstructed for the Camarda Basin (Fig. 5), suggests that the estimated incision rate of 0.25 ± 0.02 mm/a is reliable.

This incision rate is calculated at 3 km from the PAG trace (Fig. 9), thus representing a fraction of the higher rate that would be expected in closer proximity to the PAG. To consider the increasing difference in elevation approaching the fault, by projecting the correlated terrace flight onto the fault plane trace at an elevation of 21 m (Figs. 9 and 12), a minimum throw rate of 0.44 ± 0.04 mm/a was estimated for the PAG. This rate, obtained over the last 200 ka, is similar to the throw rate

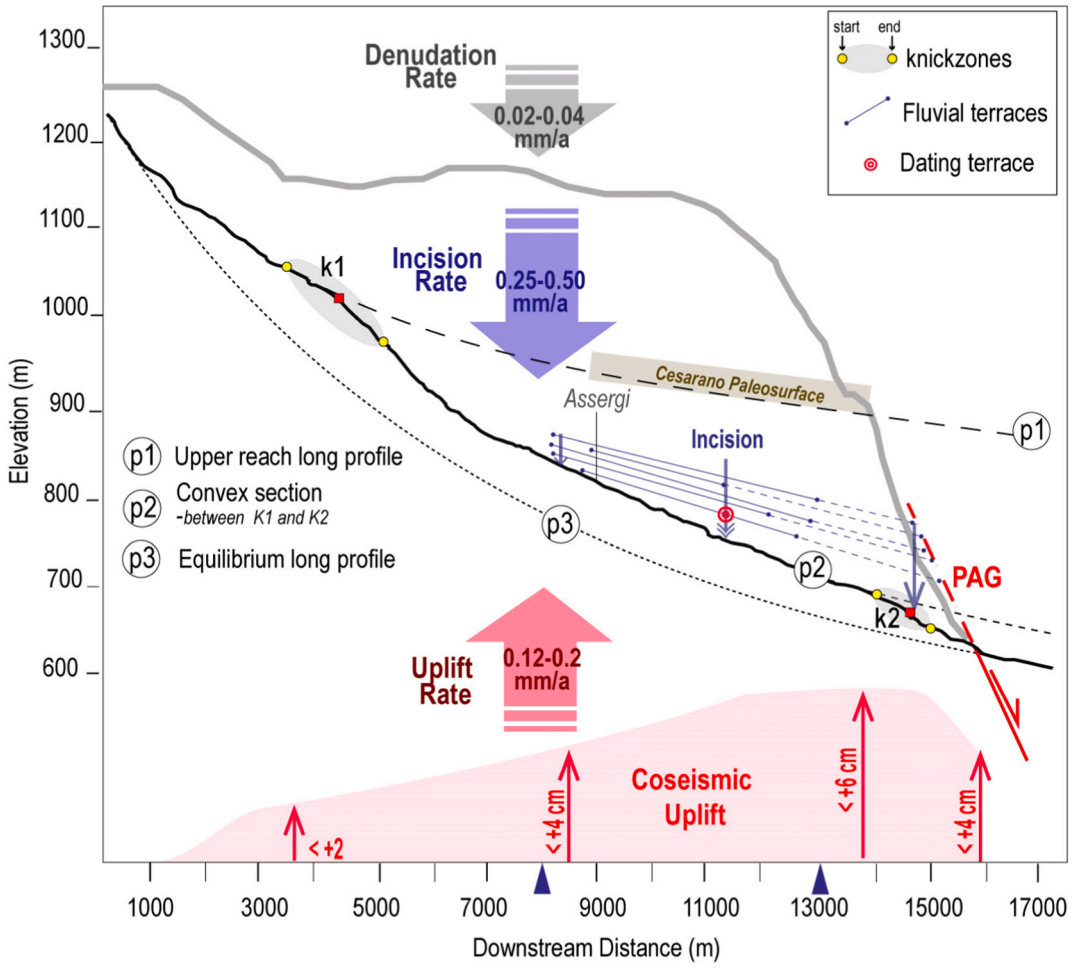

Fig. 12. Conceptual sketch of the Paganica Fault footwall evolution (vertical exaggeration) showing the competition between local tectonic forcing, incision, and denudation rate along the Raiale River longitudinal profile. The upper reach long profile is p1, derived by the concave equilibrium profile from the portion up to k1, and it coincides with the Cesarano paleovalley. The convex section p2, is related to the longitudinal profile portion between the two knickzones. The equilibrium profile p3, is derived by interpolating the profile shape at the hanging-wall of the PAG and the starting point of the Raiale River (0 m downstream distance). The denudation rate comes from the TCN method; the incision rate derives from fluvial terrace analysis; the profile of the coseismic vertical dislocation along the Raiale River is derived from the DInSAR data of Atzori et al. (2009); Fig. 13); the uplift rate is based on the coseismic uplift (up to 6.0 cm) over the average recurrence time (300–500 years, from paleoseismological data) (see the text for explanation).

suggested by Galli et al. (2010) during the last 0.5 Ma, whilst being higher than the range of rates (0.1–0.4 mm/a) found for the PSDFS over time scales of 10^4–10^6 ka (Pucci et al., 2019). Nevertheless, the value falls within the range of most of the published data on Apennines faults, that show values generally below 1.0 mm/a (Roberts and Michetti, 2004; Cinti et al., 2019), with some exceptions such as 1.3 mm/a for the Magnola Fault (Benedetti et al., 2013).

4.6. Landscape dynamics

The long-term (last 300 ka from cosmogenic ^{36}Cl nuclides) denudation rate of 0.02–0.04 mm/a calculated for the area is similar to the current denudation rate estimates on limestone for inland areas of northern Italy (i.e., 0.01–0.03 mm/a in Furlani et al., 2009) and the Mediterranean region (e.g., 0.03 mm/a in Siame et al., 2004), which have been correlated only to precipitation rates (Ryb et al., 2014). Moreover, these cosmogenic erosion rates, similar to those from upland landscapes in cool temperate climates (Heimsath et al., 2001; Phillips et al., 2006; Gunnell et al., 2013), are comparable to or slightly lower than average erosion rates from cosmogenic ^{10}Be concentrations in river sediments crossing land surfaces or in tectonically stable areas (Olivetti et al., 2012).

The presence of the fault does not seem to influence the variation of these denudation rate values, which are small compared to the magnitude order differences observed for the fault slip rate (factor of 10^{-2}; see Section 2). The summit denudation is much slower than the incision of the Raiale River valley. This is due to the slow retreat of knickzones (e.g., k1) and associated upland transmission of the transient response to the perturbations. In fact, in the study area, the landscape adjustment to a change in boundary conditions is still ongoing after 1.0 Ma, in the range of periods that may last thousands to millions of years, as observed worldwide (Di Biase et al., 2015). Consequently, such low upland erosion rates are crucial in ensuring the survival of remnant landscapes preserved at low-relief high elevations (e.g., Anzano Plateau in Fig. 2).

In the context of the study area, the dynamic equilibrium between topography and tectonics appears to not have been reached. Consequently, the landscape evolution of the PAG footwall in response to the tectonic activity is dominated by relief growth, since the Raiale Valley incision rate is one order of magnitude higher than the nearby summit denudation rate (0.25 mm/a vs. 0.03 mm/a). Thus, the incision is not equaled by the denudation, depicting a non-steady state of the topography (Fig. 12). Moreover, along with the Early–Middle Pleistocene climatic transition, the increase in fault-related relief progressively intensified the sediment and water supply to the local base level (i.e.,

Paganica-San Demetrio Basin), playing a role in the drainage integration through overspill mechanisms (Geurts et al., 2020).

Generally, this result confirms that dynamic equilibrium conditions are not met. However, its attainment could be possible considering the scale of the study area (i.e., topographic changes are scale-dependent and not precluded at the local scale of observation <100 km^2 or at time scales smaller than the significant climatic cycles of $<10^5$ years; e.g., Tucker and Whipple, 2002; Whipple and Tucker, 1999; Baldwin et al., 2003).

4.7. Paganica Fault coseismic behavior and its long-term expression

Each coseismic uplift of the PAG footwall (i.e., instantaneous perturbation produced by an individual seismic event) produces a transient wave of regressive erosion that tends to grade the longitudinal river profile by propagating knickzones. If the transient erosion wave is tectonically controlled, the knickpoint k2 and convex section (p2) indicate a persistent perturbation of the present-day Raiale River longitudinal profile. Specifically, the knickpoint suggests that during the interseismic periods after each coseismic uplift, the Raiale River cannot return to the former equilibrium profile gradient to reach a steady-state downcutting because of short earthquake recurrence time and/or large individual coseismic displacements.

Notably, the 2009 L'Aquila earthquake produced surface faulting with of ~15 cm and a coseismic dislocation field, measured using remote sensing data (Atzori et al., 2009), with a maximum footwall uplift of up to ~6 cm coinciding with the Raiale River valley long-term downcutting (Fig. 13). In this context, the 0.25–0.50 mm/a incision rate would be able to compensate for the 0.12–0.2 mm/a derived from the 2009-like seismic events occurring on the PAG with a recurrence time interval of 300–500 years (derived from 60 mm coseismic uplift from InSAR data and interevent time intervals from paleoseismological data). This suggests that the present-day anomaly of the Raiale River longitudinal profile, if of tectonic origin, would be produced by events larger than the L'Aquila one (as those documented by paleoseismological investigations with $M > 6.5$ and ~0.5 m of throw per event) and not by footwall uplift related to seismic events similar to the 2009 earthquake. Conversely, such an uplift rate due to PAG activity would not be compensated by the 0.02–0.04 mm/a denudation rate at the summit. As a result, a progressive tectonic increment of the summits absolute elevation (i.e., relief growth) occurs at the PAG footwall. (Fig. 12).

5. Conclusions

In this study, the footwall of the Paganica normal fault, the source of the 2009 Mw 6.1 L'Aquila earthquake in the Central Apennines, was investigated through integrated geological and geomorphological approaches and chronological data to extract constraints on active tectonics by taking advantage of the Raiale River that orthogonally crosscuts the fault trace. In particular, this work aimed to unravel the

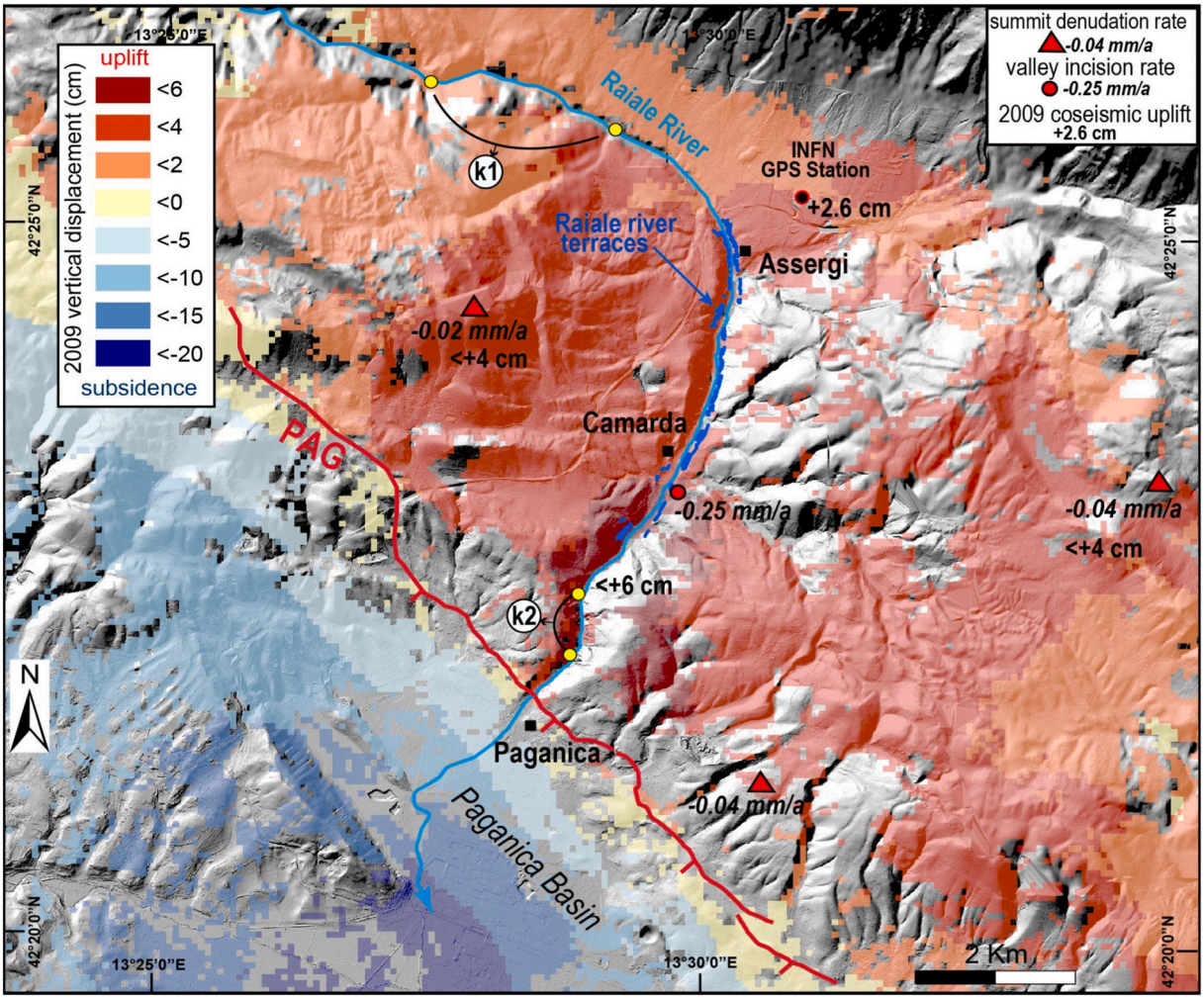

Fig. 13. Vertical component of the 2009 coseismic observed displacement field from Envisat interferograms (Atzori et al., 2009) and the GPS station of INFN recorded an uplift of 2.6 cm (Anzidei et al., 2009). The footwall uplift maximum (6 cm) coincides with the portion of the Raiale River long profile corresponding with the p2 profile.

contribution of the Paganica normal fault activity in building the landscape and reconstruct its long-term throw rate by estimating and comparing denudation and incision rates at its footwall block.

Through morphostratigraphy and paleomagnetic analysis, we outlined the Plio–Pleistocene morphotectonic evolution of the area by reconstructing the spatially limited Camarda Basin infill with its unconformity-bounded continental deposits and their relationships with faults. An initial phase of basin development was recognized that predates the Raiale River gorge's incision, controlled by dominant E–W trending faults in the Late Pliocene–Early Pleistocene and disconnected from the present-day Middle Aterno drainage. The following Early Pleistocene phase is characterized by shaping and depositional draping of the wide NE–SW-trending Cesarano paleovalley, forming the early connection between the Assergi and the Paganica Basins. Afterwards, during the Late Early Pleistocene–Middle Pleistocene, dissection of the Cesarano paleosurface commences with inset E–W-elongated paleosurfaces (i.e., Cesarano plain). At the end of this phase, the proto-Raiale River starts to markedly incise into these paleolandscapes, probably caused by ongoing activity of the Paganica Fault that progressively lowered the Raiale River base level. Up to the Holocene, the Raiale River strongly deepens its valley, recorded by a flight of fluvial terrace levels.

Detailed mapping of the Raiale River valley, along with absolute dating, allowed us to distinguish five levels of Middle–Late Pleistocene fluvial terraces, from which paleolongitudinal profiles were constructed, diverging downstream and depicting a footwall uplift gradient as approaching the Paganica Fault, consistent with long-term normal fault displacement. Consequently, we interpreted the calculated 0.25 ± 0.02 mm/a incision rate as a minimum value for the near-fault footwall uplift, where it can reach a throw rate of ~0.45 mm/a, in agreement with independent estimates derived from the literature.

In parallel, through terrestrial cosmogenic nuclides, in 0.02–0.04 mm/a, the denudation rate on the summit of the footwall block was calculated to be much slower than the incision of the Raiale River valley. This result depicts a non-steady state of the fault footwall topography, suggesting that dynamic equilibrium between topography and tectonics has not been reached; hence, a dominant relief growth is expected.

In this context, the present-day longitudinal profile of the Raiale River denotes an ungraded status, presenting two main knickzones. The upper one results from the headward propagating incision wave affecting the Cesarano paleosurface at the end of the Early Pleistocene and triggered by the Paganica Fault, showing an average migration rate in the order of 12 mm/a. The lower one, upstream of which the diverging paleolongitudinal profiles are located, suggests a younger tectonic perturbation.

Finally, considering the 2009 L'Aquila earthquake coseismic dislocation field, it was observed that the Raiale River incision rate estimated herein would be able to compensate for the maximum coseismic footwall uplift if derived from 2009-like seismic events. This suggests that the present-day anomaly of the Raiale River longitudinal profile, if it is a transience of tectonic origin, would have been produced by larger events ($M > 6.5$) as those documented in the area by paleoseismological investigations.

This study provides an important example that demonstrates the usefulness of landform markers provided by interdisciplinary approaches of Quaternary geology, morphostratigraphy, and drainage analysis in quantifying post-orogenic tectonic forcing in the Apennines and its resulting landscape response. It illustrates the role of the activity of the Paganica Fault by discriminating the landscape response to its footwall block dislocation, which is accommodated by river adjustment, depositional/erosional processes and fault-controlled basins.

Finally, the results confirm that in the Apennines, the condition of dynamic equilibrium is often not met, and that the persistence of transient perturbations induced by tectonics deserves consideration.

Declaration of competing interest

The authors declare that they have no known competing financial interests or personal relationships that could have appeared to influence the work reported in this paper.

Data availability

Data will be made available on request.

Acknowledgments

The work was financially supported by the MIUR (Italian Ministry of Education, University and Research) project “FIRB Abruzzo - High-resolution analyses for assessing the seismic hazard and risk of the areas affected by the 6 April 2009 earthquake”, ref. RBAP10ZC8K_005 and RBAP10ZC8K_007, and by Agreement INGV-DPC 2012-2021. The airborne LiDAR survey performedby the Civil Protection of Friuli Venezia Giulia (Italy) was kindly released by Italian Civil Protection Department Special thanks to Simone Atzori, who provided the InSAR data. Thanks to Riccardo Civico, Deborah Di Naccio, and Ari Matmon for the valuable discussions in the field and Chiara Caricchi for her help during the paleomagnetic analysis at the INGV laboratory in Rome. We also thank Martin Stokes, Alexander Whittaker, Alessandra Ascione and an anonymous reviewer for their useful and perceptive comments that helped to improve the clarity and quality of the paper.

Appendix A. Supplementary data

Supplementary data to this article can be found online at https://doi.org/10.1016/j.geomorph.2022.108411.

References

Adamoli, L., Calamita, F., Pizzi, A., Ispra, 2012. Note illustrative della Carta Geologica d’Italia alla scala 1: 50,000, Foglio 349, Gran Sasso d’Italia. Servizio Geologico d’Italia.

Ahnert, F., 1994. Equilibrium, scale and inheritance in geomorphology. Geomorphology 11 (2), 125–140.

Aitken, M.J., 1982. Thermoluminescence dating: past progress and future trends. Nucl. Tracks Radiat. Meas. 10 (1-2), 3–6 (1985).

Angelino, A., Bianchi Fasani, G., Bozzano, F., Colasanto, F., Colombi, A., Di Filippo, M., Verrubbi, V., 2010. Macroarea 8 (Poggio Roio, Colle Roio, Roio Piano, S. Rufina Contrada Cavalli). In: Gruppo di Lavoro MS-AQ (Ed.), Microzonazione Sismica delle macroaree. Microzonazione Sismica per la ricostruzione dell’area Aquilana. Regione Abruzzo-Presidenza del Consiglio dei Ministri, Dipartimento della Protezione Civile, L’Aquila.

Anzidei, M., Boschi, E., Cannelli, V., Devoti, R., Esposito, A., Galvani, A., Melini, D., Pietrantonio, G., Riguzzi, F., Sepe, V., Serpelloni, E., 2009. Coseismic deformation of the destructive April 6, 2009, L’Aquila earthquake (central Italy) from GPS data. Geophys. Res. Lett. 36, 1–5. https://doi.org/10.1029/2009GL039145.

Atzori, S., Hunstad, I., Chini, M., Salvi, S., Tolomei, C., Bignami, C., Stramondo, S., Trasatti, E., Antonioli, A., Boschi, E., 2009. Finite fault inversion of DInSAR coseismic displacement of the 2009 L’Aquila earthquake (central Italy). Geophys. Res. Lett. 36, 1–6. https://doi.org/10.1029/2009GL039293.

Azañón, J.M., Azor, A., Pérez-Peña, J.V., Carrillo, J.M., 2005. Late Quaternary large-scale rotational slides induced by river incision: the Arroyo de Gor area (Guadix basin, SE Spain). Geomorphology 69 (1–4), 152–168.

Bagh, S., Chiaraluce, L., De Gori, P., Moretti, M., Govoni, A., Chiarabba, C., Romanelli, M., 2007. Background seismicity in the Central Apennines of Italy: the Abruzzo region case study. Tectonophysics 444 (1–4), 80–92.

Bagnaia, R., D’epifanio, A., Sylos Labini, S., 1992. Aquila and Subequan basins: an example of Quaternary evolution in Central Apennines, Italy. Quat. Nova 2, 187–209.

Balasco, M., Galli, P., Giocoli, A., Gueguen, E., Lapenna, V., Perrone, A., Piscitelli, S., Rizzo, E., Romano, G., Siniscalchi, A., Votta, M., 2011. Deep geophysical electromagnetic section across the middle Aterno Valley (central Italy): preliminary results after the April 6, 2009, L’Aquila earthquake. Boll. Geofis. Teor. Appl. 52, 443–455. https://doi.org/10.4430/bgta0028.

Baldwin, J.A., Whipple, K.W., Tucker, G.E., 2003. Implications of the shear stress river incision model for the timescale of post-orogenic decay of topography. J. Geophys. Res. 108 (B3) https://doi.org/10.1029/2001JB000550.

Benedetti, L., Manighetti, I., Gaudemer, Y., Finkel, R., Malavieille, J., Pou, K., Arnold, M., Aumaître, G., Bourlès, D., Keddadouche, K., 2013. Earthquake synchrony and clustering on Fucino faults (Central Italy) as revealed from in situ36Cl exposure

dating. J. Geophys. Res. Solid Earth 118, 4948–4974. https://doi.org/10.1002/jgrb.50299.
Berlin, M.M., Anderson, R.S., 2007. Modeling of knickpoint retreat on the Roan Plateau, western Colorado. J. Geophys. Res. Earth Surf. 112 (F3).
Bertini, T., Bosi, C., 1993. La tettonica quaternaria della conca di Fossa (L'Aquila). Il Quaternario 6 (2), 293–314.
Blumetti, A.M., Guerrieri, L., Vittori, E., 2013. The primary role of the Paganica-San Demetrio fault system in the seismic landscape of the Middle Aterno Valley basin (Central Apennines). Quat. Int. 288, 183–194. https://doi.org/10.1016/j.quaint.2012.04.040.
Blumetti, A.M., Di Manna, P., Comerci, V., Guerrieri, L., Vittori, E., 2017. Paleoseismicity of the san demetrio ne'Vestini fault (L'Aquila basin, Central Italy): implications for seismic hazard. Quat. Int. 451, 129–142.
Bogaart, P.W., Van Balen, R.T., 2000. Numerical modeling of the response of alluvial rivers to Quaternary climate change. Glob. Planet. Chang. 27 (1–4), 147–163.
Boncio, P., Lavecchia, G., Milana, G., Rozzi, B., 2004a. Seismogenesis in Central Apennines, Italy: an integrated analysis of minor earthquake sequences and structural data in the Amatrice-Campotosto area. Ann. Geophys. 47, 1723–1742. https://doi.org/10.4401/ag-7227.
Boncio, P., Lavecchia, G., Pace, B., 2004b. Defining a model of 3D seismogenic sources for Seismic Hazard Assessment applications: the case of central Apennines (Italy). J. Seismol. 8, 407–425. https://doi.org/10.1023/B:JOSE.0000038449.78801.05.
Boncio, P., Pizzi, A., Brozzetti, F., Pomposo, G., Lavecchia, G., Di Naccio, D., Ferrarini, F., 2010. Coseismic ground deformation of the 6 April 2009 L'Aquila earthquake (central Italy, M w 6.3). Geophys. Res. Lett. 37 https://doi.org/10.1029/2010GL042807 n/a-n/a.
Bosi, C., Galadini, F., Giaccio, B., Messina, P., Sposato, A., 2003. Plio-Quaternary continental deposits in the Latium-Abruzzi Apennines: the correlation of geological events across different intermontane basins. Il Quaternario 16, 55–76.
Bøtter-Jensen, L., Bulur, E., Duller, G.A.T., Murray, A.S., 2000. Advances in luminescence instrument systems. Radiat. Meas. 32, 523–528.
Bridgland, D., Westaway, R., 2008. Climatically controlled river terrace staircases: a worldwide Quaternary phenomenon. Geomorphology 98 (3–4), 285–315.
Bull, W.B., 2008. Tectonic Geomorphology of Mountains: A New Approach to Paleoseismology. John Wiley & Sons.
Bull, W.B., 2011. Tectonically Active Landscapes. John Wiley & Sons.
Carafa, M.M., Bird, P., 2016. Improving deformation models by discounting transient signals in geodetic data: 2. Geodetic data, stress directions, and long-term strain rates in Italy. J. Geophys. Res. Solid Earth 121 (7), 5557–5575.
Carminati, E., Doglioni, C., 2012. Alps vs. apennines: the paradigm of a tectonically asymmetric Earth. Earth-Sci. Rev. 112, 67–96. https://doi.org/10.1016/j.earscirev.2012.02.004.
Cavinato, G.P., Celles, P.D., 1999. Extensional basins in the tectonically bimodal central Apennines fold-thrust belt, Italy: response to corner flow above a subducting slab in retrograde motion. Geology 27 (10), 955–958.
Centamore, E., Crescenti, U., Dramis, F., Bigi, S., Fumanti, F., Rusciadelli, G., Petitta, M., 2006. Note illustrative della Carta Geologica d'Italia alla scala 1: 50.000, Foglio 359 l'Aquila. Servizio Geologico d'Italia-Apat 128.
Cesi, C., Di Filippo, M., Di Nezza, M., Ferri, F., 2010. Caratteri gravimetrici della media Valle del Fiume Aterno. In: Gruppo di Lavoro MS-AQ (Ed.), Geologia e Pericolosità Sismica dell'area Aquilana. Microzonazione Sismica per la ricostruzione dell'area Aquilana.
Chadima, M., Hrouda, F., Melichar, R., 2006. Magnetic fabric study of the SE Rhenohercynian Zone (Bohemian Massif): Implications for dynamics of the Paleozoic accretionary wedge. Tectonophysics 418 (1–2), 93–109.
Chiarabba, C., Jovane, L., DiStefano, R., 2005. A new view of italian seismicity using 20 years of instrumental recordings. Tectonophysics 395 (3–4), 251–268.
Chiaraluce, L., 2012. Unravelling the complexity of Apenninic extensional fault systems: a review of the 2009 L'Aquila earthquake (Central Apennines, Italy). J. Struct. Geol. 42, 2–18.
Choi, J.H., Kim, J.W., Murray, A.S., Hong, D.G., Chang, H.W., Cheonga, C.S., 2009. OSL dating of marine terrace sediments on the southeastern coast of Korea with implications for Quaternary tectonics. Quat. Int. 199 (1–2), 3–14.
Chorley, R.J., Kennedy, B.A., 1971. Physical Geography: A Systems Approach. Prentice Hall.
Cinti, F.R., De Martini, P.M., Pantosti, D., Baize, S., Smedile, A., Villani, F., Brunori, C.A., 2019. 22-kyr-long record of surface faulting along the source of the 30 October 2016 earthquake (Central Apennines, Italy), from integrated paleoseismic data sets. J. Geophys. Res. Solid Earth 124 (8), 9021–9048.
Cinti, F.R., Pantosti, D., De Martini, P.M., Pucci, S., Civico, R., Pierdominici, S., Cucci, L., Brunori, C.A., Pinzi, S., Patera, A., 2011. Evidence for surface faulting events along the Paganica fault prior to the 6 April 2009 L'Aquila earthquake (central Italy). J. Geophys. Res. Solid Earth 116, 1–21. https://doi.org/10.1029/2010JB007988.
Civico, R., Pucci, S., De Martini, P.M., Pantosti, D., 2015. Morphotectonic analysis of the long-term surface expression of the 2009 L'Aquila earthquake fault (Central Italy) using airborne LiDAR data. Tectonophysics 644, 108–121. https://doi.org/10.1016/j.tecto.2014.12.024.
Civico, R., Sapia, V., Di Giulio, G., Villani, F., Pucci, S., Baccheschi, P., Pantosti, D., 2017. Geometry and evolution of a fault-controlled Quaternary basin by means of TDEM and single-station ambient vibration surveys: the example of the 2009 L'Aquila earthquake area, Central Italy. J. Geophys. Res. Solid Earth 122 (3), 2236–2259.
Coltorti, M., Consoli, M., Dramis, F., Gentili, B., Pambianchi, G., 1991. Evoluzione geomorfologica delle piane alluvionali delle Marche centro-meridionali. Geogr. Fis. Din. Quat. 14 (1), 87–100.
Cyr, A.J., Granger, D.E., Olivetti, V., Molin, P., 2010. Quantifying rock uplift rates using channel steepness and cosmogenic nuclide–determined erosion rates: examples from northern and southern Italy. Lithosphere 2 (3), 188–198.
D'Agostino, N., Jackson, J.A., Dramis, F., Funiciello, R., 2001. Interactions between mantle upwelling, drainage evolution and active normal faulting: an example from the Central Apennines (Italy). Geophys. J. Int. 147, 475–497. https://doi.org/10.1046/j.1365-246X.2001.00539.x.
D'Agostino, N., Mantenuto, S., D'Anastasio, E., Giuliani, R., Mattone, M., Calcaterra, S., Gambino, P., Bonci, L., 2011. Evidence for localized active extension in the central Apennines (Italy) from global positioning system observations. Geology 39, 291–294. https://doi.org/10.1130/G31796.1.
De Gelder, G., Fernández-Blanco, D., Melnick, D., Duclaux, G., Bell, R.E., Jara-Muñoz, J., Lacassin, R., 2019. Lithospheric flexure and rheology determined by climate cycle markers in the Corinth Rift. Sci. Rep. 9 (1), 1–12.
Devoti, R., Esposito, A., Pietrantonio, G., Pisani, A.R., Riguzzi, F., 2011. Evidence of large scale deformation patterns from GPS data in the italian subduction boundary. Earth Planet. Sci. Lett. 311 (3–4), 230–241.
Di Biase, R.A., Whipple, K.X., Lamb, M.P., Heimsath, A.M., 2015. The role of waterfalls and knickzones in controlling the style and pace of landscape adjustment in the western San Gabriel Mountains, California. Bulletin 127 (3–4), 539–559.
Dunai, T.J., 2010. Cosmogenic Nuclides: Principles, Concepts and Applications in the Earth Surface Sciences. Cambridge University Press.
Emergeo Working Group, 2009. Rilievi geologici di terreno effettuati nell'area epicentrale della sequenza sismica dell'Aquilano del 6 aprile 2009.
Fifield, L.K., Ophel, T.R., Allan, G.L., Bird, J.R., Davie, R.F., 1990. Accelerator mass spectrometry at the Australian National University's 14UD accelerator: experience and developments. Nucl. Instrum. Methods Phys. Res., Sect. B 52 (3–4), 233–237.
Furlani, S., Cucchi, F., Forti, F., Rossi, A., 2009. Comparison between coastal and inland Karst limestone lowering rates in the northeastern Adriatic Region (Italy and Croatia). Geomorphology 104 (1–2), 73–81.
Galadini, F., Galli, P., 2000. Active tectonics in the Central Apennines (Italy) – input data for seismic hazard assessment. Nat. Hazards 22, 225–270. https://doi.org/10.1023/A:1008149531980.
Galli, P., Galadini, F., Pantosti, D., 2008. Twenty years of paleoseismology in Italy. Earth-Sci. Rev. 88, 89–117. https://doi.org/10.1016/j.earscirev.2008.01.001.
Galli, P., Giaccio, B., Messina, P., 2010. The 2009 Central Italy earthquake seen through 0.5 Myr-long tectonic history of the L'Aquila faults system. Quat. Sci. Rev. 29, 3768–3789. https://doi.org/10.1016/j.quascirev.2010.08.018.
Galli, P.A., Giaccio, B., Messina, P., Peronace, E., Zuppi, G.M., 2011. Palaeoseismology of the L'Aquila faults (central Italy, 2009, M w 6.3 earthquake): implications for active fault linkage. Geophys. J. Int. 187 (3), 1119–1134.
Ge.Mi.Na, 1963. In: ILTE (Ed.), Ligniti e torbe dell'Italia continentale, p. 319. Torino IP.
Geurts, A.H., Whittaker, A.C., Gawthorpe, R.L., Cowie, P.A., 2020. Transient landscape and stratigraphic responses to drainage integration in the actively extending central Italian Apennines. Geomorphology 353, 107013.
Giaccio, B., Galli, P., Messina, P., Peronace, E., Scardia, G., Sottili, G., Sposato, A., Chiarini, E., Jicha, B., Silvestri, S., 2012. Fault and basin depocentre migration over the last 2 Ma in the L'Aquila 2009 earthquake region, central Italian Apennines. Quat. Sci. Rev. 56, 69–88. https://doi.org/10.1016/j.quascirev.2012.08.016.
Giraudi, C., 2005. Middle to late Holocene glacial variations, periglacial processes and alluvial sedimentation on the higher Apennine massifs (Italy). Quat. Res. 64 (2), 176–184.
Godard, V., Ollivier, V., Bellier, O., Miramont, C., Shabanian, E., Fleury, J., ASTER Team, 2016. Weathering-limited hillslope evolution in carbonate landscapes. Earth Planet. Sci. Lett. 446, 10–20.
Gunnell, Y., Jarman, D., Braucher, R., Calvet, M., Delmas, M., Leanni, L., Keddaouche, K., 2013. The granite tors of Dartmoor, Southwest England: rapid and recent emergence revealed by late Pleistocene cosmogenic apparent exposure ages. Quat. Sci. Rev. 61, 62–76.
Hancock, G.S., Anderson, R.S., 2002. Numerical modeling of fluvial strath-terrace formation in response to oscillating climate. Geol. Soc. Am. Bull. 114 (9), 1131–1142.
Harkins, N., Kirby, E., Heimsath, A., Robinson, R., Reiser, U., 2007. Transient fluvial incision in the headwaters of the Yellow River, northeastern Tibet, China. J. Geophys. Res. Earth Surf. 112 (F3).
Head, M.J., Gibbard, P.L., 2015. Early-Middle Pleistocene transitions: linking terrestrial and marine realms. Quat. Internat. 389, 7–46.
Heimsath, A.M., Dietrich, W.E., Nishiizumi, K., Finkel, R.C., 2001. Stochastic processes of soil production and transport: erosion rates, topographic variation and cosmogenic nuclides in the Oregon Coast Range. Earth Surf. Process. Landf. 26 (5), 531–552.
Herrmann, R.B., Malagnini, L., Munafò, I., 2011. Regional moment tensors of the 2009 L'Aquila earthquake sequence. Bull. Seismol. Soc. Am. 101 (3), 975–993.
Hetzel, R., Niedermann, S., Tao, M., Kubik, P.W., Ivy-Ochs, S., Gao, B., Strecker, M.R., 2002. Low slip rates and long-term preservation of geomorphic features in Central Asia. Nature 417 (6887), 428–432.
Hippolyte, J.C., Brocard, G., Tardy, M., Nicoud, G., Bourlès, D., Braucher, R., Souffaché, B., 2006. The recent fault scarps of the Western Alps (France): tectonic surface ruptures or gravitational sackung scarps? A combined mapping, geomorphic, levelling, and 10Be dating approach. Tectonophysics 418 (3–4), 255–276.
Hunstad, I., Selvaggi, G., D'agostino, N., England, P., Clarke, P., Pierozzi, M., 2003. Geodetic strain in peninsular Italy between 1875 and 2001. Geophys. Res. Lett. 30 (4).
Improta, L., Villani, F., Bruno, P.P., Castiello, A., Rosa, D.De, Varriale, F., Punzo, M., Brunori, C.A., Civico, R., Pierdominici, S., Berlusconi, A., Giacomuzzi, G., 2012. High-resolution controlled-source seismic tomography across the Middle Aterno basin in the epicentral area of the 2009, Mw 6.3, L'Aquila earthquake (central

Apennines, Italy). Ital. J. Geosci. 131, 373–388. https://doi.org/10.3301/IJG.2011.35.
Kirby, E., Whipple, K., 2001. Quantifying differential rock-uplift rates via stream profile analysis. Geoloy 29 (5), 415–418.
Kirby, E., Whipple, K.X., 2012. Expression of active tectonics in erosional landscapes. J. Struct. Geol. 44, 54–75. https://doi.org/10.1016/j.jsg.2012.07.009.
Lavé, J., Avouac, J.P., 2001. Fluvial incision and tectonic uplift across the Himalayas of Central Nepal. J. Geophys. Res. Solid Earth 106 (B11), 26561–26591.
Lavecchia, G., Ferrarini, F., Brozzetti, F., De Nardis, R., Boncio, P., Chiaraluce, L., 2012. From surface geology to aftershock analysis: constraints on the geometry of the L'Aquila 2009 seismogenic fault system. Ital. J. Geosci. 131 (3), 330–347.
Lisiecki, L.E., Raymo, M.E., 2005. A Pliocene-Pleistocene stack of 57 globally distributed benthic δ18O records. Paleoceanography 20, 1–17. https://doi.org/10.1029/2004PA001071.
Macrì, P., Smedile, A., Speranza, F., Sagnotti, L., Porreca, M., Mochales, T., Ermolli, E.R., 2016. Analysis of a 150 m sediment core from the co-seismic subsidence depocenter of the 2009 Mw= 6.1 L'Aquila earthquake (Italy): implications for Holocene-Pleistocene tectonic subsidence rates and for the age of the seismogenic Paganica fault system. Tectonophysics 687, 180–194.
Merritts, D., Vincent, K.R., 1989. Geomorphic response of coastal streams to low, intermediate, and high rates of uplift, Medocino triple junction region, northern California. Geol. Soc. Am. Bull. 101 (11), 1373–1388.
Messina, P., Moro, M., Speranza, F., 2001. Primi risultati di stratigrafia magnetica su alcune formazioni continentali dell'alta Valle dell'Aterno (Italia centrale). Il Quaternario 14, 167–172.
Moro, M., Gori, S., Falcucci, E., Saroli, M., Galadini, F., Salvi, S., 2013. Historical earthquakes and variable kinematic behaviour of the 2009 L'Aquila seismic event (central Italy) causative fault, revealed by paleoseismological investigations. Tectonophysics 583, 131–144. https://doi.org/10.1016/j.tecto.2012.10.036.
Murray, A.S., Wintle, A.G., 2003. The single aliquot regenerative dose protocol: potential for improvements in reliability. Radiat. Meas. 37 (4–5), 377–381.
Nesci, O., Savelli, D., Troiani, F., 2012. Types and development of stream terraces in the Marche Apennines (central Italy): a review and remarks on recent appraisals. Géomorphologie Relief Processus Environ. 18 (2), 215–238.
Nocentini, M., Cosentino, D., Spadi, M., Tallini, M., 2018. Plio-Quaternary geology of the Paganica-San Demetrio-Castelnuovo Basin (Central Italy). J. Maps 14 (2), 411–420.
Olivetti, V., Cyr, A.J., Molin, P., Faccenna, C., Granger, D.E., 2012. Uplift history of the Sila Massif, southern Italy, deciphered from cosmogenic 10Be erosion rates and river longitudinal profile analysis. Tectonics 31 (3).
Pace, B., Peruzza, L., Lavecchia, G., Boncio, P., 2006. Layered seismogenic source model and probabilistic seismic-hazard analyses in Central Italy. Bull. Seismol. Soc. Am. 96 (1), 107–132.
Papanikolaou, I.D., Foumelis, M., Parcharidis, I., Lekkas, E.L., Fountoulis, I.G., 2010. Deformation pattern of the 6 and 7 April 2009, M W= 6.3 and M W= 5.6 earthquakes in L'Aquila (Central Italy) revealed by ground and space-based observations. Nat. Hazards Earth Syst. Sci. 10 (1), 73–87.
Pazzaglia, F.J., 2003. Landscape evolution models. Dev. Quat. Sci. 1, 247–274.
Pazzaglia, F.J., Gardner, T.W., Merritts, D.J., 1998. Bedrock fluvial incision and longitudinal profile development over geologic time scales determined by fluvial terraces. Geophys. Monogr. 107, 207–236.
Pérez-Peña, J.V., Azañón, J.M., Azor, A., Tuccimei, P., Della Seta, M., Soligo, M., 2009. Quaternary landscape evolution and erosion rates for an intramontane Neogene basin (Guadix–Baza basin, SE Spain). Geomorphology 106 (3–4), 206–218.
Pérez-Peña, J.V., Azor, A., Azañón, J.M., Keller, E.A., 2010. Active tectonics in the Sierra Nevada (Betic Cordillera, SE Spain): Insights from geomorphic indexes and drainage pattern analysis. Geomorphology 119 (1–2), 74–87.
Peruzza, L., Pace, B., Visini, F., 2011. Fault-based earthquake rupture forecast in Central Italy: remarks after the L'Aquila M w 6.3 event. Bull. Seismol. Soc. Am. 101 (1), 404–412.
Phillips, W.M., Hall, A.M., Mottram, R., Fifield, L.K., Sugden, D.E., 2006. Cosmogenic 10Be and 26Al exposure ages of tors and erratics, Cairngorm Mountains, Scotland: timescales for the development of a classic landscape of selective linear glacial erosion. Geomorphology 73 (3–4), 222–245.
Pizzi, A., Calamita, F., Coltorti, M., Pieruccini, P., 2002. Quaternary normal faults, intramontane basins and seismicity in the Umbria-Marche-Abruzzi Apennine Ridge (Italy): contribution of neotectonic analysis to seismic hazard assessment. Boll. Soc. Geol. Ital. 1, 923–929.
Pondrelli, S., Salimbeni, S., Morelli, A., Ekstr, G., Olivieri, M., Boschi, E., 2009. In: Earthquake Sequence, 0, pp. 238–242. https://doi.org/10.1111/j.1365-246X.2009.04418.x.
Pondrelli, S., Salimbeni, S., Morelli, A., Ekström, G., Olivieri, M., Boschi, E., 2010. Seismic moment tensors of the April 2009, L'Aquila (Central Italy), earthquake sequence. Geophys. J. Int. 180 (1), 238–242.
Porreca, M., Smedile, A., Speranza, F., Mochales, T., Caracciolo, F.D.A., Di Giulio, G., Sagnotti, L., 2016. Geological reconstruction in the area of maximum co-seismic subsidence during the 2009 Mw= 6.1 L'Aquila earthquake using geophysical and borehole data. Ital. J. Geosci. 135 (2), 350–362.
Pucci, S., Mirabella, F., Pazzaglia, F., Barchi, M.R., Melelli, L., Tuccimei, P., Soligo, M., Saccucci, L., 2014. Interaction between regional and local tectonic forcing along a complex Quaternary extensional basin: Upper Tiber Valley, Northern Apennines, Italy. Quat. Sci. Rev. 102, 111–132. https://doi.org/10.1016/j.quascirev.2014.08.009.
Pucci, S., Villani, F., Civico, R., Pantosti, D., Del Carlo, P., Smedile, A., De Martini, P.M., Pons-Branchu, E., Gueli, A., 2015. Quaternary geology of the Middle Aterno Valley, 2009 L'Aquila earthquake area (Abruzzi Apennines, Italy). J. Maps 11, 689–697. https://doi.org/10.1080/17445647.2014.927128.
Pucci, S., Civico, R., Villani, F., Ricci, T., Delcher, E., Finizola, A., Sapia, V., De Martini, P.M., Pantosti, D., Barde-Cabusson, S., Brothelande, E., Gusset, R., Mezon, C., Orefice, S., Peltier, A., Poret, M., Torres, L., Suski, B., 2016. Deep electrical resistivity tomography along the tectonically active Middle Aterno Valley (2009 L'Aquila earthquake area, Central Italy). Geophys. J. Int. 207, 967–982. https://doi.org/10.1093/gji/ggw308.
Pucci, S., Villani, F., Civico, R., Di Naccio, D., Porreca, M., Benedetti, L., Pantosti, D., 2019. Complexity of the 2009 L'Aquila earthquake causative fault system (Abruzzi Apennines, Italy) and effects on the Middle Aterno Quaternary basin arrangement. Quat. Sci. Rev. 213, 30–66.
Roberts, G.P., Michetti, A.M., 2004. Spatial and temporal variations in growth rates along active normal fault systems: an example from the Lazio-Abruzzo Apennines, Central Italy. J. Struct. Geol. 26, 339–376. https://doi.org/10.1016/S0191-8141(03)00103-2.
Roberts, G.P., Raithatha, B., Sileo, G., Pizzi, A., Pucci, S., Walker, J.F., Walters, R., 2010. Shallow subsurface structure of the 2009 April 6 M w 6.3 L'Aquila earthquake surface rupture at Paganica, investigated with ground-penetrating radar. Geophys. J. Int. 183 (2), 774–790.
Roberts, H.M., 2006. Optical dating of coarse-silt sized quartz from loess: evaluation of equivalent dose determinations and SAR procedural checks. Radiat. Meas. 41, 923–929.
Rovida, A.N., Locati, M., Camassi, R.D., Lolli, B., Gasperini, P., 2016. CPTI15, the 2015 Version of the Parametric Catalogue of Italian Earthquakes.
Ryb, U., Matmon, A., Erel, Y., Haviv, I., Benedetti, L., Hidy, A.J., 2014. Styles and rates of long-term denudation in carbonate terrains under a Mediterranean to hyper-arid climatic gradient. Earth Planet. Sci. Lett. 406, 142–152. https://doi.org/10.1016/j.epsl.2014.09.008.
Santo, A., Ascione, A., Di Crescenzo, G., Miccadei, E., Piacentini, T., Valente, E., 2014. Tectonic-geomorphological map of the middle Aterno River valley (Abruzzo, Central Italy). J. Maps 10, 365–378. https://doi.org/10.1080/17445647.2013.867545.
Saroli, M., Moro, M., Florindo, F., Lancia, M., Lurcock, P.C., Dinarès-Turell, J., 2015. Paleomagnetic dating of tectonically influenced Plio-Quaternary fan-system deposits from the Apennines (Italy). Ann. Geophys. 58, 1–5. https://doi.org/10.4401/ag-6740.
Schimmelpfennig, I., Benedetti, L., Finkel, R., Pik, R., Blard, P.H., Bourlès, D., Burnard, P., Williams, A., 2009. Sources of in-situ 36Cl in basaltic rocks. Implications for calibration of production rates. Quat. Geochronol. 4, 441–461. https://doi.org/10.1016/j.quageo.2009.06.003.
Schimmelpfennig, I., Benedetti, L., Garreta, V., Pik, R., Blard, P.H., Burnard, P., Bourles, D., Finkel, R., Ammon, K., Dunai, T., 2011. Calibration of cosmogenic ^{36}Cl production rates from Ca and K spallation in lava flows from Mt. Etna (38 N, Italy) and Payun Matru (36 S, Argentina). Geochimica et Cosmochimica Acta 75 (10), 2611–2632.
Schumm, S.A., 1993. River response to baselevel change: implications for sequence stratigraphy. J. Geol. 101 (2), 279–294.
Schwanghart, W., Scherler, D., 2014. TopoToolbox 2–MATLAB-based software for topographic analysis and modeling in Earth surface sciences. Earth Surf. Dyn. 2 (1), 1–7.
Scognamiglio, L., Tinti, E., Michelini, A., Dreger, D.S., Cirella, A., Cocco, M., Mazza, S., Piatanesi, A., 2010. Fast Determination of Moment Tensors and Rupture history: what has been Learned from the 6 April 2009 L'Aquila Earthquake Sequence. Seismol. Res. Lett. 81, 892–906. https://doi.org/10.1016/S0169-4332(96)00754-4.
Sharma, P., Kubik, P.W., Fehn, U., Gove, H.E., Nishiizumi, K., Elmore, D., 1990. Development of 36Cl standards for AMS. Nucl. Instrum. Methods Phys. Res., Sect. B 52 (3–4), 410–415.
Siame, L., Bellier, O., Braucher, R., Sébrier, M., Cushing, M., Bourlès, D., Yiou, F., 2004. Local erosion rates versus active tectonics: cosmic ray exposure modelling in Provence (south-East France). Earth Planet. Sci. Lett. 220 (3–4), 345–364.
Snyder, N.P., Hodges, K.V., 2000. Depositional and tectonic evolution of a supradetachment basin: 40Ar/39Ar geochronology of the Nova Formation, Panamint Range, California. Basin Res. 12 (1), 19–30.
Spadi, M., Gliozzi, E., Cosentino, D., Nocentini, M., 2016. Late Piacenzian-Gelasian freshwater ostracods (Crustacea) from the L'Aquila Basin (central Apennines, Italy). J. Syst. Palaeontol. 14 (7), 617–642.
Starkel, L., 2003. Climatically controlled terraces in uplifting mountain areas. Quat. Sci. Rev. 22 (20), 2189–2198.
Stone, J.O., 2000. Air pressure and cosmogenic isotope production. J. Geophys. Res. Solid Earth 105 (B10), 23753–23759.
Tallini, M., Cavuoto, G., Del Monaco, F., Di Fiore, V., Mancini, M., Caielli, G., Rapolla, A., 2012. Seismic surveys integrated with geological data for in-depth investigation of Mt. Pettino active Fault area (Western L'Aquila Basin). Ital. J. Geosci. 131 (3), 389–402.
Tarquini, S., Vinci, S., Favalli, M., Doumaz, F., Fornaciai, A., Nannipieri, L., 2012. Release of a 10-m-resolution DEM for the italian territory: comparison with global-coverage DEMs and anaglyph-mode exploration via the web. Comput. Geosci. 38 (1), 168–170.
Terulliani, A., Rossi, A., Cucci, L., Vecchi, M., 2009. L'Aquila (central Italy) earthquakes: The predecessors of the April 6, 2009 event. Seis. Res. Lett. 60 (6), 1008–1013.
Tucker, G.E., Whipple, K.X., 2002. In: Topographic Outcomes Predicted by Stream Erosion Models: Sensitivity Analysis and Intermodel Comparison, 107, pp. 1–16. https://doi.org/10.1029/2001JB000162.
Valoroso, L., Chiaraluce, L., Piccinini, D., Di Stefano, R., Schaff, D., Waldhauser, F., 2013. Radiography of a normal fault system by 64,000 high-precision earthquake locations: the 2009 L'Aquila (central Italy) case study. J. Geophys. Res. Solid Earth 118 (3), 1156–1176.

Vannoli, P., Burrato, P., Fracassi, U., Valensise, G., 2012. A fresh look at the seismotectonics of the Abruzzi (Central Apennines) following the 6 April 2009 L'Aquila earthquake (Mw 6.3). Ital. J. Geosci. 131 (3), 309–329.

Villani, F., Tulliani, V., Sapia, V., Fierro, E., Civico, R., Pantosti, D., 2015. Shallow subsurface imaging of the Piano di Pezza active normal fault (central Italy) by high-resolution refraction and electrical resistivity tomography coupled with time-domain electromagnetic data. Geophys. Suppl. Month. Notices R. Astron. Soc. 203 (3), 1482–1494.

Villani, F., Improta, L., Pucci, S., Civico, R., Bruno, P.P.G., Pantosti, D., 2017. Investigating the architecture of the Paganica Fault (2009Mw6.1 earthquake, Central Italy) by integrating high-resolution multiscale refraction tomography and detailed geological mapping. Geophys. J. Int. 208, 403–423. https://doi.org/10.1093/gji/ggw407.

Watchman, A.L., Twidale, C.R., 2002. Relative and 'absolute'dating of land surfaces. Earth Sci. Rev. 58 (1–2), 1–49.

Wegmann, K.W., Pazzaglia, F.J., 2009. Late Quaternary fluvial terraces of the Romagna and Marche Apennines, Italy: climatic, lithologic, and tectonic controls on terrace genesis in an active orogen. Quat. Sci. Rev. 28 (1–2), 137–165.

Whipple, K.X., Tucker, G.E., 1999. In: Dynamics of the Stream-power River Incision Model: Implications for Height Limits of Mountain Ranges, Landscape Response Timescales, and Research Needs, 104, pp. 661–674.

Whipple, K.X., Tucker, G.E., 2002. Implications of sediment-flux-dependent river incision models for landscape evolution. J. Geophys. Res. Solid Earth 107 (B2), ETG–3. https://doi.org/10.1029/2001JB000162.

Whittaker, A.C., Boulton, S.J., 2012. Tectonic and climatic controls on knickpoint retreat rates and landscape response times. J. Geophys. Res. 117, F02024.

Whittaker, A.C., Cowie, P.A., Attal, M., Tucker, G.E., Roberts, G.P., 2007. Contrasting transient and steady-state rivers crossing active normal faults: New field observations from the Central Apennines, Italy. Basin Res. 19 (4), 529–556.

Whittaker, A.C., Cowie, P.A., Attal, M., Tucker, G.E., Roberts, G.P., 2007a. Bedrock channel adjustment to tectonic forcing: implications for predicting river incision rates. Geology 35, 103–106. https://doi.org/10.1130/G23106A.1.

Whittaker, A.C., Attal, M., Cowie, P.A., Tucker, G.E., Roberts, G., 2008. Decoding temporal and spatial patterns of fault uplift using transient river long profiles. Geomorphology 100, 506–526. https://doi.org/10.1016/j.geomorph.2008.01.018.

Whittaker, A.C., Attal, M., Allen, P.A., 2010. Characterising the origin, nature and fate of sediment exported from catchments perturbed by active tectonics. Basin Res. 22 (6), 809–828.

Willeit, M., Ganopolski, A., Calov, R., Brovkin, V., 2019. Mid-Pleistocene transition in glacial cycles explained by declining CO2 and regolith removal. Sci. Adv. 5 (4), eaav7337.

Wobus, C., Whipple, K.X., Kirby, E., Snyder, N., Johnson, J., Spyropolou, K., Willett, S.D., 2006. Tectonics from topography: procedures, promise, and pitfalls. Spec. Pap. Geol. Soc. Am. 398, 55.

Zhang, J.Y., Liu-Zeng, J., Scherler, D., Yin, A., Wang, W., Tang, M.Y., Li, Z.F., 2018. Spatiotemporal variation of late Quaternary river incision rates in Southeast Tibet, constrained by dating fluvial terraces. Lithosphere 10 (5), 662–675.

Zhou, M., Xia, J., Lu, J., Deng, S., Lin, F., 2017. Morphological adjustments in a meandering reach of the middle Yangtze River caused by severe human activities. Geomorphology 285, 325–332.